IMA Journal of Applied Mathematics (2021) **00**, 1–48
https://doi.org/10.1093/imamat/hxab040

Behaviour of solutions to the 1D focusing stochastic L^2-critical and supercritical nonlinear Schrödinger equation with space-time white noise

Annie Millet
Statistique, Analyse et Modélisation Multidisciplinaire (SAMM, EA 4543), Université Paris 1, 90 Rue de Tolbiac, 75013 Paris Cedex, France and Laboratoire de Probabilités, Statistique et Modélisation (LPSM, UMR 8001), Bâtiment Sophie Germain, Université de Paris, France

and

Svetlana Roudenko* and Kai Yang
Department of Mathematics and Statistics, Florida International University, Miami, FL 33199, USA
*Corresponding author: sroudenko@fiu.edu

[Received on 28 May 2020; revised on 17 June 2021; accepted on 20 August 2021]

We study the focusing stochastic nonlinear Schrödinger equation in 1D in the L^2-critical and supercritical cases with an additive or multiplicative perturbation driven by space-time white noise. Unlike the deterministic case, the Hamiltonian (or energy) is not conserved in the stochastic setting nor is the mass (or the L^2-norm) conserved in the additive case. Therefore, we investigate the time evolution of these quantities. After that, we study the influence of noise on the global behaviour of solutions. In particular, we show that the noise may induce blow up, thus ceasing the global existence of the solution, which otherwise would be global in the deterministic setting. Furthermore, we study the effect of the noise on the blow-up dynamics in both multiplicative and additive noise settings and obtain profiles and rates of the blow-up solutions. Our findings conclude that the blow-up parameters (rate and profile) are insensitive to the type or strength of the noise: if blow up happens, it has the same dynamics as in the deterministic setting; however, there is a (random) shift of the blow-up centre, which can be described as a random variable normally distributed.

Keywords: stochastic NLS; space-time white noise; additive noise; multiplicative noise; blow-up dynamics; mass-conservative numerical schemes.

1. Introduction

We consider the 1D focusing stochastic nonlinear Schrödinger (SNLS) equation, i.e. the NLS equation subject to a random perturbation f

$$\begin{cases} iu_t + u_{xx} + |u|^{2\sigma}u = \epsilon f(u), \quad (x,t) \in [0,\infty) \times \mathbb{R}, \\ u(0,x) = u_0(x). \end{cases} \tag{1.1}$$

Here, the term $f(u)$ stands for a stochastic perturbation driven by a space-time white noise $W(dt,dx)$ (described in Section 2.1) and $u_0 \in H^1(\mathbb{R})$ is the deterministic initial condition. In this paper, we study the SNLS equation (1.1) with either an additive or a multiplicative perturbation driven by space-time white noise: its effect on the mass (L^2 norm) and energy (Hamiltonian), the influence of the noise on the global behaviour of solutions and, in particular, its effect on the blow-up dynamics. In the

deterministic setting, the mass and the energy are typically conserved; however, these quantities may behave differently under stochastic perturbations, which might significantly change global behaviour of solutions.

The focusing stochastic NLS equation appears in physical models that involve random media, inhomogeneities or noisy sources. For example, the influence of the additive noise on the soliton propagation is studied in Falkovich *et al.* (2001), multiplicative noise in the context of Scheibe aggregates is discussed in Rasmussen *et al.* (1995), the NLS studies in random media (via the inverse scattering transform) are discussed in Garnier (1998) and Abdullaev & Garnier (2005) (and references therein). Relevant analytical studies of the SNLS (1.1) have been done by de Bouard & Debussche (2002a,b, 2003, 2005) and numerical investigations by Barton-Smith *et al.* (2005) and Debussche & Di Menza (2002a,b).

We consider two cases of the stochastic perturbation $f(u)$ in (1.1):

$$f(u) = \begin{cases} u(x,t) \circ W(dt,dx), & \text{multiplicative case,} \\ W(dt,dx), & \text{additive case.} \end{cases} \tag{1.2}$$

The notation $u(x,t) \circ W(dt,dx)$ stands for the Stratonovich integral, which makes sense when the noise is more regular (e.g. when W is replaced by its approximation W_N). This integral can be related to the Itô integral (using the Stratonovich–Itô correction term); for more details, we refer the reader to de Bouard & Debussche (2003, pp. 99–100). The reason for the Stratonovich integral is the mass conservation, which we discuss next while recalling the properties of the deterministic NLS equation.

The deterministic case of (1.1), corresponding to $\epsilon = 0$, has been intensively studied in the past several decades. The local well-posedness in H^1 goes back to the works of Ginibre & Velo (1979, 1985); see also Kato (1987), Tsutsumi (1987), Cazenave & Weissler (1990) and Cazenave (2003) for further details. During their lifespans, solutions to the deterministic equation (1.1) conserve several quantities, which include the mass $M(u)$ and the energy (or Hamiltonian) $H(u)$ defined as

$$M(u(t)) = \|u(t)\|_{L^2}^2 \equiv M(u_0) \quad \text{and} \quad H(u(t)) = \frac{1}{2}\|\nabla u(t)\|_{L^2}^2 - \frac{1}{2\sigma+2}\|u(t)\|_{L^{2\sigma+2}}^{2\sigma+2} \equiv H(u_0).$$

The deterministic equation is invariant under the scaling: if $u(t,x)$ is a solution to (1.1) with $\epsilon = 0$, then so is $u_\lambda(t,x) = \lambda^{1/\sigma}\, u(\lambda^2 t, \lambda x)$. This scaling makes the Sobolev $\dot{H}^s$ norm of the solution invariant with the scaling index s defined as

$$s = \frac{1}{2} - \frac{1}{\sigma}. \tag{1.3}$$

Thus, the 1D quintic ($\sigma = 2$) NLS is called the L^2-critical equation ($s = 0$). The nonlinearities higher than quintic (or $\sigma > 2$) make the NLS equation L^2-supercritical ($s > 0$)[1] ; when $\sigma < 2$, the equation is L^2-subcritical.

In this work, we mostly study the L^2-critical and supercritical SNLS equation (1.1) with quintic or higher powers of nonlinearity. In these cases, it is known that H^1 solutions may not exist globally in

[1] The range of the critical index in 1D is $0 < s < \frac{1}{2}$.

time (and thus, blow up in finite time), which can be shown by a well-known convexity argument on a finite variance (Vlasov *et al.*, 1970; Zakharov, 1972; for a review, see Sulem & Sulem, 1999). We next recall the notion of standing waves, i.e. solutions to the deterministic NLS of the form $u(t,x) = e^{it}Q(x)$. Here, Q is a smooth positive decaying at infinity solution to

$$-Q + Q'' + Q^{2\sigma+1} = 0. \tag{1.4}$$

This solution is unique and is called the ground state (see Weinstein, 1982/83, and references therein). In 1D, this solution is explicit: $Q(x) = (1+\sigma)^{\frac{1}{2\sigma}}\ \mathrm{sech}^{\frac{1}{\sigma}}(\sigma x)$.

In the L^2-critical case ($\sigma = 2$), the threshold for globally existing vs. finite time existing solutions was first obtained by Weinstein (1982/83), showing that if $M(u_0) < M(Q)$, then the solution $u(t)$ exists globally in time[2] ; otherwise, if $M(u_0) \geq M(Q)$, the solution $u(t)$ may blow up in finite time. The minimal mass blow-up solutions (with mass equal to $M(Q)$) would be nothing else but the pseudoconformal transformations of the ground state solution $e^{it}Q$ by the result of Merle (1993). While these blow-up solutions are explicit, they are unstable under perturbations. The known stable blow-up dynamics is available for solutions with the initial mass larger than that of the ground state Q and has a rich history, see Yang *et al.* (2018), Yang *et al.* (2020), Sulem & Sulem (1999) and Fibich (2015) (and references therein); the key features are recalled later.

In the L^2-supercritical case ($s > 0$), the known thresholds for globally existing vs. blow up in finite time solutions depend on the scale-invariant quantities such as $\mathcal{ME}(u) := M(u)^{1-s}H(u)^s$ and $\|u\|_{L^2}^{1-s}\|\nabla u(t)\|_{L^2}^s$, where the former is conserved in time and the latter changes the L^2-norm of the gradient. The original dichotomy was obtained in the fundamental work by Kenig & Merle (2006) in the energy-critical case ($s = 1$ in dimensions 3,4,5), where they introduced the concentration compactness and rigidity approach to show the scattering behaviour (i.e. approaching a linear evolution) for the globally existing solutions under the energy threshold (i.e. $H(u_0) < H(Q)$ in the energy-critical setting). It was extended to the intercritical case $0 < s < 1$ in Holmer & Roudenko (2007), Duyckaerts *et al.* (2008) and Guevara (2014), followed by many other adaptations to various evolution equations and settings. A combined result for $0 \leq s \leq 1$ is the following theorem (here, $X = \{H^1$ if $0 < s < 1$; L^2 if $s = 0$; $\dot{H}^1$ if $s = 1\}$, for simplicity stated for zero momentum).

THEOREM 1 (Dodson, 2015; Duyckaerts *et al.*, 2008; Fang *et al.*, 2011; Guevara, 2014; Holmer & Roudenko, 2007, 2008, 2010; Kenig & Merle, 2006). Let $u_0 \in X(\mathbb{R}^N)$ and $u(t)$ be the corresponding solution to the deterministic NLS equation (1.1) ($\epsilon = 0$) with the maximal interval of existence (T_*, T^*). Suppose that $M(u_0)^{1-s}H(u_0)^s < M(Q)^{1-s}H(Q)^s$.

- If $\|u_0\|_{L^2}^{1-s}\|\nabla u_0\|_{L^2}^s < \|Q\|_{L^2}^{1-s}\|\nabla Q\|_{L^2}^s$, then $u(t)$ exists for all $t \in \mathbb{R}$ with $\|u(t)\|_{L^2}^{1-s}\|\nabla u(t)\|_{L^2}^s < \|Q\|_{L^2}^{1-s}\|\nabla Q\|_{L^2}^s$ and $u(t)$ scatters in X: there exist $u_\pm \in X(\mathbb{R}^N)$ such that $\lim_{t\to\pm\infty} \|u(t) - e^{it\Delta}u_\pm\|_{X(\mathbb{R}^N)} = 0$.
- If $\|u_0\|_{L^2}^{1-s}\|\nabla u_0\|_{L^2}^s > \|Q\|_{L^2}^{1-s}\|\nabla Q\|_{L^2}^s$, then $\|u(t)\|_{L^2}^{1-s}\|\nabla u(t)\|_{L^2}^s > \|Q\|_{L^2}^{1-s}\|\nabla Q\|_{L^2}^s$ for $t \in (T_*, T^*)$. Moreover, if $|x|u_0 \in L^2(\mathbb{R}^N)$ (finite variance) or u_0 is radial, then the solution blows up in finite time; if u_0 is of infinite variance and non-radial ($s > 0$), then either the solution blows up in finite time or there exits a sequence of times $t_n \to +\infty$ (or $t_n \to -\infty$) such that $\|\nabla u(t_n)\|_{L^2(\mathbb{R}^N)} \to \infty$.

[2] It scatters to a linear solution in L^2, see Dodson (2015) and references therein.

The focusing NLS equation subject to a stochastic perturbation has been studied in de Bouard & Debussche (2003) in the L^2-subcritical case, showing a global well-posedness for any $u_0 \in H^1$. Blow-up for $0 \leq s < 1$ has been studied in de Bouard & Debussche (2002b) for an additive perturbation and de Bouard & Debussche (2005) for a multiplicative noise. The results in de Bouard & Debussche (2005) state that in the multiplicative noise case for $s \geq 0$ initial conditions with finite (analytic) variance and sufficiently negative energy blow up before some finite time $t > 0$ with positive probability (de Bouard & Debussche, 2002b, Theorem 4.1). For both additive and multiplicative noise, in the L^2-supercritical case, the authors prove that if noise is non-degenerate and regular enough and the initial condition u_0 is different from 0, then blow up happens with positive probability before a given fixed time $t > 0$ (see further details in de Bouard & Debussche, 2002b, Theorem 1.2, which also discusses the L^2-critical situation in the additive case, and de Bouard & Debussche, 2005, Theorem 5.1). This differs from the deterministic setting, where no blow up occurs for initial data strictly smaller than the ground state (in terms of the mass). The additive noise NSL models are used in fibre optic communication systems to transfer bits of information (aka solitons), the limitations on the bit rate and error-free transmission distances are set mainly by the spontaneous emission noise added by in-line optical amplifiers; see e.g. Falkovich *et al.* (2001). An important role is then played by theoretical methods to evaluate systems performance and specific transmission of a signal along fibre lines, even if it gets distorted and disappears or gets absorbed by the overall noise, and the time and rate how fast it happens. Therefore, in this work, we also investigate the additive noise setting for the above applications.

In Millet & Roudenko (2021), an adaptation of the above Theorem 1 is obtained to understand the global behaviour of solutions in the stochastic setting in the L^2-critical and supercritical cases. One major difference is that mass and energy are not necessarily conserved in the stochastic setting. In the SNLS equation with multiplicative noise (defined via Stratonovich integral), the mass is conserved a.s. (see de Bouard & Debussche, 2003), which allows to prove global existence of solutions in the L^2-critical setting with $M(u_0) < M(Q)$ (see Millet & Roudenko, 2021). (A somewhat similar situation happens in the additive noise case, though mass is no longer conserved and actually grows linearly in time (see (2.10)). To understand global behaviour in the L^2-supercritical setting, one needs to control energy (as can be seen from Theorem 1). While it is possible to obtain some upper bounds on the energy on a (random) time interval (and in the additive noise it is also necessary to localize the mass on a random set, since it is not conserved), the exact behaviour of energy is not clear. This is exactly what we investigate in this paper via discretization of both quantities (mass and energy) in various contexts, then obtaining estimates on the discrete analogs and tracking the dependence on several parameters. Once we track the growth (and levelling off in the multiplicative case) of energy (and mass in the additive setting), we study the global behaviour of solutions. In particular, we investigate the blow-up dynamics of solutions in both L^2-critical and supercritical settings and obtain the rates, profiles and other features such as a location of blow up. Before we state these findings, we review the blow up in the deterministic setting. For more details, review and history of the problem, e.g. see the work of the second and third authors (Yang *et al.*, 2018, 2019), Sulem & Sulem (1999) and Fibich (2015).

A stable blow up in deterministic setting exhibits a self-similar structure with a specific rate and profile. Investigations of stable blow up go back to 1970s for the cubic NLS in two and three dimensions. In 2D, the NLS equation is L^2-critical, and the rate of how fast the blow-up forms has been a long-time enterprise both numerically and analytically. When the mass of the initial data is close to that of the soliton, the questions have been settled, but for arbitrarily large mass the analytical studies are yet to produce. The profile of the self-similar blow up in this case is given by a rescaled version of the ground state Q and the rate has the so-called loglog correction. In 3D, the NLS is L^2-supercritical, and while numerically the dynamics has been investigated, the analytical description is not yet available due to

the analytical description of the profile, e.g. see Yang *et al.* (2019), Sulem & Sulem (1999) and Fibich (2015). The rate in the supercritical case is nevertheless understood. We now provide more details on the description of the blow up in both cases. Thanks to the scaling invariance, the following rescaling of the (deterministic) equation is introduced via the new space and time coordinates (τ, ξ) and a scaling function $L(t)$ (for more details, see LeMesurier *et al.*, 1987; Sulem & Sulem, 1999; Yang *et al.*, 2019)

$$u(t,r) = \frac{1}{L(t)^{\frac{1}{\sigma}}} v(\tau,\xi), \quad \text{where} \quad \xi = \frac{r}{L(t)}, \quad r = |x|, \quad \tau = \int_0^t \frac{\mathrm{d}s}{L(s)^2}. \tag{1.5}$$

Then the equation (1.1) in the deterministic setting ($\epsilon = 0$) becomes

$$iv_\tau + ia(\tau)\left(\xi v_\xi + \frac{v}{\sigma}\right) + \Delta v + |v|^{2\sigma} v = 0 \tag{1.6}$$

with

$$a(\tau) = -L\frac{dL}{dt} \equiv -\frac{d\ln L}{d\tau}. \tag{1.7}$$

The limiting behaviour of $a(\tau)$ as $\tau \to \infty$ (from the second term in (1.6)) creates a significant difference in blow-up behaviour between the L^2-critical and L^2-supercritical cases. As $a(\tau)$ is related to $L(t)$ via (1.7), the behaviour of the rate, $L(t)$, is typically studied to understand the blow-up behaviour. Separating variables $v(\tau,\xi) = e^{i\tau}Q(\xi)$ in (1.6) and assuming that $a(\tau)$ converges to a constant a, the following problem is studied to gain information about the blow-up profile:

$$\begin{cases} \Delta_\xi Q - Q + ia\left(\dfrac{Q}{\sigma} + \xi Q_\xi\right) + |Q|^{2\sigma} Q = 0, \\ Q_\xi(0) = 0, \qquad Q(0) = \text{real}, \qquad Q(\infty) = 0. \end{cases} \tag{1.8}$$

Besides the conditions above, it is also required to have $|Q(\xi)|$ decrease monotonically with ξ, without any oscillations as $\xi \to \infty$ (see more on that in Budd *et al.*, 1999; Sulem & Sulem, 1999; Yang *et al.*, 2019). In the L^2-critical case, the above equation is simplified (due to a being zero) to the ground state equation (1.4). However, even in that critical context, the equation (1.8) is still meticulously investigated (with non-zero a but asymptotically approaching zero), since the correction in the blow-up rate $L(t)$ comes exactly from that. It should be emphasized that the decay of $a(\tau)$ to zero in the critical case is extremely slow, which makes it very difficult to pin down the exact blow-up rate, or more precisely, the correction term in the blow-up rate, and it was quite some time until rigorous analytical proofs appeared (in 1D, Perelman, 2000, followed by a systematic work from Merle & Raphael, 2005a, to Merle & Raphael, 2005b; see review in Introduction of Yang *et al.*, 2019, or Fibich, 2015; Sulem & Sulem, 1999). In the L^2-supercritical case, the convergence of $a(\tau)$ to a non-zero constant is rather fast, and the rescaled solution converges to the blow-up profile fast as well. The more difficult question in this case is the profile itself, since it is no longer the ground state from (1.4) but exactly an admissible solution (without fast oscillating decay and with an asymptotic decay of $|\xi|^{-\frac{1}{\sigma}}$ as $|\xi| \to \infty$) of (1.8).

Among all admissible solutions to (1.8), there is no uniqueness as it was shown in Budd *et al.* (1999), Kopell & Landman (1995) and Yang *et al.* (2019). These solutions generate branches of so-called multi-bump profiles that are labelled $Q_{J,K}$, indicating that the Jth branch converges to the Jth excited state,

and K is the enumeration of solutions in a branch. The solution $Q_{1,0}$, the first solution in the branch $Q_{1,K}$ (this is the branch, which converges to the L^2-critical ground state solution Q in (1.4) as the critical index $s \to 0$), is shown (numerically) to be the profile of stable supercritical blow up. The second and third authors have been able to obtain the profile $Q_{1,0}$ in various NLS cases (see Yang *et al.*, 2019, also an adaptation for a non-local Hartree-type NLS, Yang *et al.*, 2020), and thus, we are able to use that in this work and compare it with the stochastic case.

In the focusing SNLS case, in Debussche & Di Menza (2002a) and Debussche & Di Menza (2002b), numerical simulations are done when the driving noise is rough, namely, it is an approximation of space-time white noise. The effect of the additive and multiplicative noise is described for the propagation of solitary waves. In particular, it was noted that the blow-up mechanism transfers energy from the larger scales to smaller scales, thus, allowing the mesh size to affect the formation of the blow up in the multiplicative noise case (the coarse mesh allows formation of blow up and the finer mesh prevents it or delays it). The probability of the blow-up time is also investigated and found that in the multiplicative case it is delayed on average. In the additive noise case (where noise is acting as the constant injection of energy), the blow up seems to be amplified and happens sooner on average, for further details refer to Debussche & Di Menza (2002b, Section 4). Other parameters' dependence (such as on the strength ϵ of the noise) is also discussed. We note that the observed behaviour of solutions as noted highly depends on the discretization and numerical scheme used.

In this paper, we design three numerical schemes to study the SNLS (1.1) driven by the space-time white noise. We then use these schemes to track the time dependence of mass and energy of the stochastic Schrödinger flow in each multiplicative and additive noise cases. After that, we investigate the influence of the noise on the blow-up dynamics. For the stochastic NLS equation, we pose and then investigate numerically the following conjectures.

CONJECTURE 1 (L^2-critical case). Let $u_0 \in H^1(\mathbb{R})$ and $u(t)$, $t > 0$, be an evolution of the SNLS equation (1.1) with $\sigma = 2$ and noise (1.2).

In the multiplicative (Stratonovich) noise case, sufficiently localized initial data with $\|u_0\|_{L^2} > \|Q\|_{L^2}$ blow up in finite positive (random) time with positive probability.

In the additive noise case, sufficiently localized initial data blow up in finite (random) time a.s.

If a solution blows up at a random positive time $T(\omega) > 0$ for a given $\omega \in \Omega$, then the blow up is characterized by a self-similar profile (same ground state profile Q from (1.4) as in the deterministic NLS) and for t close to $T(\omega)$

$$\|\nabla u(t,\cdot)\|_{L^2_x} \sim \frac{1}{L(t)}, \quad L(t) \sim \left(\frac{2\pi(T-t)}{\ln|\ln(T-t)|}\right)^{\frac{1}{2}} \quad \text{as} \quad t \to T = T(\omega), \tag{1.9}$$

known as the 'log-log' rate due to the double logarithmic correction in $L(t)$.

Thus, the solution blows up in a self-similar regime with a profile converging to a rescaled ground state profile Q, and the core part of the solution $u_c(x,t)$ behaves as follows:

$$u_c(t,x) \sim \frac{1}{L(t)^{\frac{1}{2}}} Q\left(\frac{x - x(t)}{L(t)}\right) e^{i\gamma(t)}$$

with parameters $L(t)$ converging as in (1.9), $\gamma(t) \to \gamma_0$, and $x(t) \to x_c$, the blow-up centre x_c.

Furthermore, conditionally on the existence of blow up in finite time $T(\omega) > 0$, x_c is a Gaussian random variable; no conditioning is necessary in the additive case.

CONJECTURE 2 (L^2-supercritical case). Let $u_0 \in H^1(\mathbb{R})$ and $u(t)$ be an evolution of the SNLS equation (1.1) with $\sigma > 2$ and noise (1.2).

In the multiplicative (Stratonovich) noise case, sufficiently localized initial data blow up in finite positive (random) time with positive probability.

In the additive noise case, any initial data lead to a blow up in finite (random) time a.s.

If a solution blows up at a random positive time $T(\omega) > 0$ for a given $\omega \in \Omega$, then the blow-up core dynamics $u_c(x,t)$ for t close to $T(\omega)$ is characterized as

$$u_c(t,x) \sim \frac{1}{L(t)^{\frac{1}{\sigma}}} Q\left(\frac{x - x(t)}{L(t)}\right) \exp\left(i\theta(t) + \frac{i}{2a(t)} \log \frac{T}{T-t}\right), \tag{1.10}$$

where the blow-up profile Q is the $Q_{1,0}$ solution of the equation (1.8), $a(t) \to a$, the specific constant corresponding to the $Q_{1,0}$ profile, $\theta(t) \to \theta_0$, $x(t) \to x_c$, the blow-up centre, and $L(t) = (2a(T-t))^{\frac{1}{2}}$. Consequently, a direct computation yields that for t close to $T(\omega)$

$$\|\nabla u(t,\cdot)\|_{L^2_x} \sim \frac{1}{L(t)^{1-s}} \equiv (2a(T-t))^{-\frac{1}{2}(\frac{1}{2}+\frac{1}{\sigma})}. \tag{1.11}$$

Furthermore, conditionally on the existence of blow up in finite time $T(\omega) > 0$, x_c is a Gaussian random variable; no conditioning is necessary in the additive case.

Thus, the blow up happens with a polynomial rate (1.11) without correction, and with profile converging to the same blow-up profile as in the deterministic supercritical NLS case.

As it was mentioned above, parts of the above conjectures concerning existence of blow up have been studied and partially confirmed in Debussche & Di Menza (2002b), Debussche & Di Menza (2002a), de Bouard & Debussche (2005) and de Bouard & Debussche (2002a) under various conditions. In this work, we provide numerical confirmation to both conjectures for various initial data (see also Debussche & Di Menza, 2002b) not only for the existence of blow-up solutions but also characteristics of blow-up solutions. We note that this paper is the first work where the dynamics of blow-up solutions such as profiles, rates and location are investigated in the stochastic setting.

The paper is organized as follows. In Section 2, we give a description of the driving noise and recall analytical estimates for mass and energy in both multiplicative and additive settings. In Section 3, we introduce three numerical schemes which are mass conservative in deterministic and multiplicative noise settings, and one of them is energy conservative in the deterministic setting. We discretize mass and energy and give theoretical upper bounds on those discrete analogs in Sections 3.3 and 3.4; this is followed by the corresponding numerical results, which track both mass and energy in various settings, and time dependence on the noise type and strength and other discretization parameters (such as length of the interval, space and time step sizes). In Section 4, we create a mesh refinement strategy and make sure that it also conserves mass before and after the refinement, introducing a new mass-interpolation method. We then state our new full algorithm for the numerical study of solutions behaviour for both deterministic and stochastic settings. We note that this algorithm is novel even in the deterministic case for studying the blow-up dynamics (typically, the dynamic rescaling or moving mesh methods are used). The new algorithm is needed due to the stochastic setting, since noise creates rough solutions, compared with the deterministic case, and thus, the previous methods are simply not applicable. In Section 5, we start considering global dynamics (e.g. of solitons, and how noise affects the soliton solutions) and compare with the previously known results in the L^2-subcritical case. Finally, in Section 6, we

study the blow-up dynamics in both the L^2-critical ($\sigma = 2$) and L^2-supercritical (e.g. $\sigma = 3$) cases. We observe that once a blow up starts to form, the noise does not seem to affect either the blow-up profile or the blow-up rate. The only effect that we have observed is random shifting of the blow-up centre of the rescaled ground state. With increasing number of runs, the variation in the centre location appears to be distributed normally (we estimate the corresponding mean, which is very close to 0, and variance). Otherwise, there seems to be very little difference between the multiplicative/additive noise and deterministic settings. We give a summary of our findings in the last section.

2. Description of noise and its effect on mass and energy

2.1 *Description of the driving noise*

The space-time white noise is defined in terms of a real-valued zero-mean Gaussian random field

$$\{W(B) \ : \ B \text{ bounded measurable subset of } [0, +\infty) \times \mathbb{R}\}$$

defined on a probability space $(\Omega, \mathcal{F}, P)$, with covariance given by

$$E\big[W(B)W(C)\big] = \int_{B\cap C} \mathrm{d}t\,\mathrm{d}x$$

for bounded measurable subsets B, C of $[0, \infty) \times \mathbb{R}$. For $t \geq 0$, let

$$\mathcal{F}_t := \sigma(W(B) : \ B \text{ bounded measurable subset of } [0, t] \times \mathbb{R}).$$

Given $0 \leq t_1 < t_2$ and a step function $h_N = \sum_{l=1}^N a_l 1_{[y_l, y_{l+1})}$, where $a_l \in \mathbb{R}$ and $y_1 < y_2 < \cdots < y_{N+1}$ are real numbers, we let $\int_{t_1}^{t_2} \int_{\mathbb{R}} h_N(x) W(\mathrm{d}s, \mathrm{d}x) := \sum_{l=1}^N a_l W([t_1, t_2] \times [y_l, y_{l+1}))$. Given $0 \leq t_1 < t_2$ and a function $h \in L^2(\mathbb{R}; \mathbb{R})$, we can define the stochastic Wiener integral $\int_{t_1}^{t_2} \int_{\mathbb{R}} h(x) W(\mathrm{d}t, \mathrm{d}x)$ as the $L^2(\Omega)$ limit of $\int_{t_1}^{t_2} \int_{\mathbb{R}} h_N(x) W(\mathrm{d}t, \mathrm{d}x)$ for any sequence of step functions h_N converging to h in $L^2(\mathbb{R}; \mathbb{R})$. This stochastic integral is a centred Gaussian random variable with variance $[t_2 - t_1] \int_{\mathbb{R}} |h(x)|^2 \mathrm{d}x$. Furthermore, if h_1, h_2 are orthogonal functions in $L^2(\mathbb{R}; \mathbb{R})$ with $\|h_1\|_{L^2} = \|h_2\|_{L^2} = 1$, the processes $\{\int_0^t h_1(x) W(\mathrm{d}t, \mathrm{d}x)\}_{t\geq 0}$ and $\{\int_0^t h_2(x) W(\mathrm{d}t, \mathrm{d}x)\}_{t\geq 0}$ are independent Brownian motions for the filtration $(\mathcal{F}_t, t \geq 0)$.

Given a non-negative integer k, let $L^{0,k}_{2,\mathbb{R}}$ denote the set of Hilbert–Schmidt operators from $L^2(\mathbb{R}; \mathbb{R}))$ to $H^k(\mathbb{R}; \mathbb{R})$, where $H^0(\mathbb{R}; \mathbb{R}) = L^2(\mathbb{R}; \mathbb{R})$. Given $\phi \in L^{0,k}_{2,\mathbb{R}}$, let $\|\phi\|_{L^{0,k}_{2,\mathbb{R}}}$ denote its Hilbert–Schmidt norm. Let $\{e_j\}_{j\geq 0}$ be an orthonormal basis of $L^2(\mathbb{R} : \mathbb{R})$ and let $\beta_j(t) = \int_0^t \int_{\mathbb{R}} e_j(x) W(\mathrm{d}s, \mathrm{d}x)$, $j \geq 0$. The processes $\{\beta_j\}$ are independent 1D Brownian motions and we can formally write

$$W(t, x, \omega) = \sum_{j\geq 0} \beta_j(t, \omega) e_j(x), \quad t \geq 0, \ x \in \mathbb{R}, \ \omega \in \Omega. \tag{2.1}$$

However, the above series does not converge in $L^2(\mathbb{R}; \mathbb{R})$ for a fixed $t > 0$. To obtain an $L^2(\mathbb{R}; \mathbb{R})$-valued Brownian motion, we should replace the space-time white noise W by a Brownian motion white in time and coloured in space. More precisely, in the above series, we should replace e_j by ϕe_j for some

operator ϕ in $L^{0,0}_{2,\mathbb{R}}$, which is a Hilbert–Schmidt operator from $L^2(\mathbb{R})$ to $L^2(\mathbb{R})$ with the Hilbert–Schmidt norm $\|\phi\|_{L^{0,0}_{2,\mathbb{R}}}$. This would yield $\tilde{W}(t) = \sum_{j\geq 0} \beta_j(t)\phi e_j$ for some sequence $\{\beta_j\}_{j\geq 0}$ of independent 1D Brownian motions and some orthonormal basis $\{e_j\}_{j\geq 0}$ of $L^2(\mathbb{R};\mathbb{R})$. The covariance operator $\mathcal{Q}$ of $\tilde{W}$ is trace-class with Trace $\mathcal{Q} = \|\phi\|^2_{L^{0,0}_{2,\mathbb{R}}}$.

For practical reasons, we will use approximations of the space-time white noise W (thus, a more regular noise) using finite sums

$$W_N(t,x,\omega) := \sum_{j=0}^{N} \beta_j(t,\omega)e_j(x), \tag{2.2}$$

with functions $\{e_j\}_j$ with disjoint supports, which are normalized in $L^2(\mathbb{R};\mathbb{R})$. This finite sum gives rise to an $L^2(\mathbb{R};\mathbb{R})$-valued Brownian motion with the covariance operator $\mathcal{Q}$ such that Trace $\mathcal{Q} = N+1$.

Unlike Debussche & Di Menza (2002a,b), we will not suppose that the functions $\{e_j\}$ are indicator functions of disjoint intervals. Instead we will consider the following 'hat' functions, which belong to H^1.

For fixed $N \geq 1$, we consider the hat functions $\{g_j\}_{0\leq j\leq N}$ defined on the space interval $[x_j, x_{j+1}]$ as follows. Let $x_{j+\frac{1}{2}} := \frac{1}{2}[x_j + x_{j+1}]$, $\Delta x_j := x_{j+1} - x_j$, and for $j = 0, \cdots N-1$, set

$$g_j(x) := \begin{cases} c_j(x - x_j) & \text{for} \quad x \in [x_j, x_{j+\frac{1}{2}}], \\ c_j(x_{j+1} - x) & \text{for} \quad x \in [x_{j+\frac{1}{2}}, x_{j+1}], \end{cases}$$

where $c_j := \frac{2\sqrt{3}}{(\Delta x_j)^{3/2}}$ is chosen to ensure $\|g_j\|_{L^2} = 1$.

Given points $x_0 < x_1 < \cdots < x_N$, define the functions $e_j, j = 0, \cdots, N$, by

$$\begin{cases} e_j = & g_{j-1}1_{[x_{j-\frac{1}{2}}, x_j]} + g_j 1_{[x_j, x_{j+\frac{1}{2}}]}, \ 1 \leq j \leq N-1, \\ e_0 = & \sqrt{2}g_0 1_{[x_0, x_{\frac{1}{2}}]}, \quad e_N = \sqrt{2}g_{N-1}1_{[x_{N-\frac{1}{2}}, x_N]}. \end{cases} \tag{2.3}$$

Due to the symmetry of the functions $\{g_j\}$, we have $\|e_j\|_{L^2} = 1$ for $j = 0, \cdots, N$. Since the functions $\{e_j\}$s have disjoint supports, they are orthogonal in $L^2(\mathbb{R};\mathbb{R})$. We can now construct an orthonormal basis $\{e_k\}_{k\geq 0}$ of $L^2(\mathbb{R};\mathbb{R})$ containing the above $\{e_j\}_{0\leq j\leq N}$ set as the first $N+1$ elements. Then the $L^{0,0}_{2,\mathbb{R}}$-Hilbert–Schmidt norm of the orthogonal projection ϕ_N from $L^2(\mathbb{R};\mathbb{R})$ to the span of $\{e_j\}_{0\leq j\leq N}$ is equal to $N+1$.

Furthermore, unlike indicator functions, the above functions $\{e_j\}$ belong to H^1. When the mesh size Δx_j is constant (equal to Δx), an easy computation yields $\|e_j\|^2_{H^1} = 1 + \frac{12}{(\Delta x)^2}$ and $\|\nabla e_j\|^2_{L^\infty} = \frac{12}{(\Delta x)^3}$. Therefore, if $\|\cdot\|_{L^{0,1}_{2,\mathbb{R}}}$ denotes the Hilbert–Schmidt norm from $L^2(\mathbb{R};\mathbb{R})$ to $H^1(\mathbb{R};\mathbb{R})$, we have

$$\|\phi_N\|^2_{L^{0,1}_{2,\mathbb{R}}} = (N+1)\Big(1 + \frac{12}{(\Delta x)^2}\Big) \sim \frac{12\,(N+1)}{(\Delta x)^2} \quad \text{when} \quad \Delta x << 1, \tag{2.4}$$

and

$$m_{\phi_N} := \sup_{x\in\mathbb{R}} \sum_{k\geq 0} \left|\nabla(\phi_N e_k)(x)\right|^2 = \frac{12\,(N+1)}{(\Delta x)^3}. \tag{2.5}$$

2.2 *Multiplicative noise*

We recall that this stochastic perturbation on the right-hand side of (1.1) is $f(u) = u(x,t) \circ W(dt,dx)$, where the multiplication understood via the Stratonovich integral, which makes sense for a more regular noise. When the noise $\tilde{W} = \sum_{j\geq 0} \beta_j \phi e_j$ is regular in the space variable (i.e. coloured in space by means of the operator $\phi \in L^{0,0}_{2,\mathbb{R}}$), the equation (1.1) conserves mass almost surely (see de Bouard & Debussche, 2003, Proposition 4.4), i.e. for any $t > 0$

$$M[u(t)] = M[u_0] \quad \text{a.s.} \tag{2.6}$$

Using the time evolution of energy in the multiplicative case for a regular noise $\tilde{W}$ (see (de Bouard & Debussche, 2003, Proposition 4.5), we have

$$\begin{aligned} H(u(t)) =& H(u_0) - \operatorname{Im}\epsilon \sum_{j\geq 0} \int_0^t \int_{\mathbb{R}} \bar{u}(s,x)\nabla u(s,x)\cdot(\nabla\phi e_j)(x)\,\mathrm{d}x\,\mathrm{d}\beta_j(s) \\ &+ \frac{\epsilon^2}{2}\sum_{j\geq 0}\int_0^t\int_{\mathbb{R}} |u(t,x)|^2\,|\nabla(\phi e_j)|^2\,\mathrm{d}x\,\mathrm{d}s. \end{aligned}$$

Taking expected values and using the fact that ϕ is Radonifying from $L^2(\mathbb{R};\mathbb{R})$ to $\dot{W}^{1,\infty}(\mathbb{R};\mathbb{R})$, we deduce that

$$\mathbb{E}(H\big(u(t)\big) = H(u_0) + \frac{\epsilon^2}{2}\,\mathbb{E}\sum_{j\geq 0}\int_0^t\int_{\mathbb{R}} |u(s,x)|^2\big|\nabla(\phi e_j)(x)\big|^2\mathrm{d}x\,\mathrm{d}s \leq H(u_0) + \frac{\epsilon^2}{2} m_\phi M(u_0)\,t, \tag{2.7}$$

where

$$m_\phi := \sup_{x\in\mathbb{R}} \sum_{j\geq 0} |\nabla(\phi e_j)(x)|^2 < \infty. \tag{2.8}$$

We also consider the expected value of the supremum in time of the energy (Hamiltonian). However, the upper bound differs depending on the critical or supercritical cases. For exact statements and notation, we refer the reader to Millet & Roudenko (2021), where it is shown that for any stopping time $\tau < \tau^*(u_0)$ (here, $\tau^*(u_0)$ is the 'random' existence time from the local theory), one has

$$\mathbb{E}\Big(\sup_{s\leq\tau} H\big(u(s)\big)\Big) \leq \mathbb{E}\big(H(u_0)\big) + \frac{\epsilon^2}{2} m_\phi\, M(u_0)\,\mathbb{E}(\tau) \;+ 3\epsilon\sqrt{m_\phi M(u_0)}\,\mathbb{E}\Big(\sqrt{\tau}\,\sup_{s\leq\tau}\|\nabla u(s)\|_{L^2(\mathbb{R}^n)}\Big).$$

Therefore, the bound on the energy depends on the growth of the last gradient term. In the L^2-critical case, assuming that $\|u_0\|_{L^2} < \|Q\|_{L^2}$, it is possible to control the kinetic energy $\|\nabla u(s)\|_{L^2}^2$ in terms of the energy $H(u)$ (see e.g. Millet & Roudenko, 2021). Therefore, $\tau^*(u_0) = +\infty$ a.s. (see Millet & Roudenko, 2021), and thus, for large times the upper estimate for the growth of the energy is at most linear: for any $t > 0$, we have

$$\mathbb{E}\Big(\sup_{s\le t} H\big(u(s)\big)\Big) \le \mathbb{E}\big(H(u_0)\big) + c_1\epsilon^2\, m_\phi M(u_0)\, t + c_2\,\epsilon\,\sqrt{m_\phi M(u_0)}\,\sqrt{t}. \tag{2.9}$$

In the L^2-supercritical case, it is more delicate to control the gradient; nevertheless, it is possible for some (random) time interval (for which we provide upper and lower bounds in Millet & Roudenko (2021). The length of that time interval is inversely proportional to the strength of the noise ϵ, the space correlation m_ϕ and the size of the initial mass $M(u_0)$ to some power depending on σ.

2.3 *Additive noise*

The additive perturbation in (1.1) is $f(u) = W(dt, dx)$. In this case, mass is no longer conserved. It is easy to see that its expected value grows linearly in time. More precisely, the identity

$$M\big(u(t)\big) = M(u_0) + \epsilon^2\|\phi\|_{L^{0,0}_{2\mathbb{R}}}^2\, t - 2\epsilon\,\mathrm{Im}\,\Big(\sum_{j=0}^{N}\int_0^t\int_{\mathbb{R}} u(s,x)\overline{\phi e_j(x)}\,\mathrm{d}x\,\mathrm{d}\beta_j(s)\Big)$$

(see e.g. de Bouard & Debussche, 2003, p. 106, or Millet & Roudenko, 2021) implies

$$\mathbb{E}(M(u(t))) = M(u_0) + \epsilon^2\|\phi\|_{L^{0,0}_{2,\mathbb{R}}}^2\, t. \tag{2.10}$$

For the energy bound, using Millet & Roudenko (2021) (see also de Bouard & Debussche, 2003, Proposition 3.3), we have

$$\begin{aligned} H(u(t)) \le & H(u_0) + \frac{\epsilon^2}{2}\tau\|\phi\|_{L^{0,1}_{2,\mathbb{R}}}^2 + \mathrm{Im}\,\epsilon\Big(\sum_{k\ge0}\int_0^\tau\int_{\mathbb{R}} \nabla\overline{u(s,x)}\nabla(\phi e_k)(x)\,\mathrm{d}x\,\mathrm{d}\beta_k(s)\Big) \\ & - \mathrm{Im}\,\epsilon\Big(\sum_{k\ge0}\int_0^\tau\int_{\mathbb{R}} |u(s,x)|^{2\sigma}\overline{u(s,x)}(\phi e_k)(x)\mathrm{d}x\,\mathrm{d}\beta_k(s)\Big). \end{aligned}$$

Taking expected values, we deduce the following 'linear' upper bound for the time evolution of the expected (instantaneous) energy

$$\mathbb{E}\big(H(u(t))\big) \le H(u_0) + \frac{\epsilon^2}{2}\|\phi\|_{L^{0,1}_{2,\mathbb{R}}}^2\, t. \tag{2.11}$$

As in the multiplicative case, in order to have quantitative information on the expected time of the existence interval, we have to prove upper bounds on $\mathbb{E}\big(\sup_{s<\tau} H(u(s))\big)$. However, since in the additive noise case the mass is not conserved and grows linearly in time, we have to localize the energy estimate on a (random) set, where the mass can be controlled (for details, see Millet & Roudenko, 2021,

Section 3). With that localization and estimates on the time, the upper bound for the expected energy is linear in time; furthermore, the time existence of solutions is inversely proportional to ϵ^2 and the correlation m_ϕ.

Next, we would like to investigate the mass and energy quantities numerically. For that, we define discretized (typically referred to as 'discrete') analogs of mass and energy, we also introduce several numerical schemes, which we use to simulate solutions, and thus, track the above quantities. We first prove theoretical upper bounds on the discrete mass and energy in both multiplicative and additive noise cases and then provide the results of our numerical simulations.

3. Numerical approach

We start with introducing our numerical schemes for the SNLS (1.1). We present three numerical schemes that conserve the discrete mass in the deterministic and with a multiplicative stochastic perturbation. Furthermore, one of them also conserves the discrete energy (in the deterministic case). That mass-energy conservative (MEC) scheme is a highly nonlinear scheme, which involves additional steps of Newton iterations, slowing down the computations significantly and generating numerical errors. We simplify that scheme first to the Crank–Nicolson (CN) scheme, which is still nonlinear, though works slightly faster. Then after that we introduce a linearized extrapolation (LE) scheme that is much faster (no Newton iterations involved) while producing tolerable errors. Before describing the schemes, we first define the finite difference operators on the non-uniform mesh.

3.1 *Discretizations*

3.1.1 *Finite difference operator on the non-uniform mesh.* We start with the description of an efficient way to approximate the space derivatives f_x and f_{xx}.

Let $\{x_j\}_{j=0}^N$ be the grid points on $[-L_c, L_c]$ (the points x_j are not necessarily equi-distributed). From the Taylor expansion of $f(x_{j-1})$ and $f(x_{j+1})$ around x_j, setting $f_j = f(x_j)$ and $\Delta x_j = x_{j+1} - x_j$, one has

$$f_x(x_j) \approx \frac{-\Delta x_j}{\Delta x_{j-1}(\Delta x_{j-1} + \Delta x_j)} f_{j-1} + \frac{\Delta x_j - \Delta x_{j-1}}{\Delta x_{j-1}\Delta x_j} f_j + \frac{\Delta x_{j-1}}{(\Delta x_{j-1} + \Delta x_j)\Delta x_j} f_{j+1}, \tag{3.1}$$

and

$$f_{xx}(x_j) \approx \frac{2}{\Delta x_{j-1}(\Delta x_{j-1} + \Delta x_j)} f_{j-1} - \frac{2}{\Delta x_{j-1}\Delta x_j} f_j + \frac{2}{(\Delta x_{j-1} + \Delta x_j)\Delta x_j} f_{j+1}. \tag{3.2}$$

We define the second-order finite difference operator

$$\mathcal{D}_2 f_j := \frac{2}{\Delta x_{j-1}(\Delta x_{j-1} + \Delta x_j)} f_{j-1} - \frac{2}{\Delta x_{j-1}\Delta x_j} f_j + \frac{2}{(\Delta x_{j-1} + \Delta x_j)\Delta x_j} f_{j+1}. \tag{3.3}$$

3.1.2 *Discretization of space, time and noise.* We denote the full discretization in both space and time by $u_j^m := u(t_m, x_j)$ at the mth time step and the jth grid point. We denote the size of a time step by $\Delta t_{m-1} = t_m - t_{m-1}$.

To consider the Stratonovich stochastic integral, we let $x_{j+\frac{1}{2}} = \frac{1}{2}[x_j + x_{j+1}]$, and we discretize the stochastic term in a way similar to that in Debussche & Di Menza (2002b), except that we use the basis $\{e_j\}_{0\le j\le N}$ defined in (2.3) instead of the indicator functions. Recall that $\{\beta_j(t)\}_{0\le j\le N}$ are the associated independent Brownian motions for the approximation W_N of the noise W (i.e. $\beta_j(t) = \int_0^t \int_{\mathbb{R}} e_j(x) W(\mathrm{d}t, \mathrm{d}x)$). Following a procedure similar to that in Debussche & Di Menza (2002b), we set

$$\chi_j^{m+\frac{1}{2}} = \frac{1}{\sqrt{\Delta t_m}}(\beta_j(t_{m+1}) - \beta_j(t_m)), \quad 0 \le j \le N.$$

We note that the random variables $\{\chi_j^{m+\frac{1}{2}}\}_{j,m}$ are independent Gaussian random variables $\mathcal{N}(0,1)$. In our simulation, the vector $(\chi_0^{m+\frac{1}{2}}, \cdots, \chi_N^{m+\frac{1}{2}})$ is obtained by the Matlab random number generator `normrnd`.

When computing a solution at the end points x_0 and x_{N+1}, we set $u_0^m = u_1^m$ and $u_N^m = u_{N-1}^m$ for all m. We also introduce the pseudo-point x_{-1} satisfying $\Delta x_{-1} = \Delta x_0$, and similarly, the pseudo-point x_{N+1} satisfying $\Delta x_{N-1} = \Delta x_N$. Let

$$f_j^{m+\frac{1}{2}} = \frac{1}{2}\big(u_j^m + u_j^{m+1}\big)\tilde{f}_j^{m+\frac{1}{2}}, \quad \text{where} \quad \tilde{f}_j^{m+\frac{1}{2}} := \frac{\sqrt{3}}{2}\frac{\big[\sqrt{\Delta x_{j-1}} + \sqrt{\Delta x_j}\big]}{\sqrt{\Delta t_m}\big[\Delta x_{j-1} + \Delta x_j\big]}\chi_j^{m+\frac{1}{2}} \tag{3.4}$$

for $j = 1, \cdots N-1$. Indeed,

$$\begin{aligned}
\tilde{f}_j^{m+\frac{1}{2}} =& \frac{2}{\Delta t_m(\Delta x_{j-1} + \Delta x_j)} \int_{t_m}^{t_{m+1}} \mathrm{d}\beta_j(s) \int_{\mathbb{R}} e_j(x)\mathrm{d}x \\
=& \frac{2}{\Delta t_m(\Delta x_{j-1} + \Delta x_j)} \big(\beta_j(t_{m+1}) - \beta_j(t_m)\big)\Big[\int_{x_{j-\frac{1}{2}}}^{x_j} c_{j-1}(x_j - x)\mathrm{d}x + \int_{x_j}^{x_{j+\frac{1}{2}}} c_j(x - x_j)\mathrm{d}x\Big] \\
=& \frac{\sqrt{3}}{2}\frac{\beta_j(t_{m+1}) - \beta_j(t_m)}{\sqrt{\Delta t_m}}\frac{\big[\sqrt{\Delta x_{j-1}} + \sqrt{\Delta x_j}\big]}{\big[\Delta x_{j-1} + \Delta x_j\big]}\chi_j^{m+\frac{1}{2}}.
\end{aligned} \tag{3.5}$$

A similar computation gives

$$f_0^{m+\frac{1}{2}} = \frac{1}{2}\big(u_0^m + u_0^{m+1}\big)\tilde{f}_0^{m+\frac{1}{2}}, \quad \text{where} \quad \tilde{f}_0^{m+\frac{1}{2}} = \frac{\sqrt{3}}{2}\frac{1}{\sqrt{\Delta t_m \Delta x_0}}\chi_0^{m+\frac{1}{2}}, \tag{3.6}$$

$$f_N^{m+\frac{1}{2}} = \frac{1}{2}\big(u_N^m + u_N^{m+1}\big)\tilde{f}_N^{m+\frac{1}{2}}, \quad \text{where} \quad \tilde{f}_N^{m+\frac{1}{2}} = \frac{\sqrt{3}}{2}\frac{1}{\sqrt{\Delta t_m \Delta x_N}}\chi_N^{m+\frac{1}{2}}. \tag{3.7}$$

Note that in the definition of $f_j^{m+\frac{1}{2}}$, the factor $\frac{1}{2}\big(u_j^m + u_j^{m+1}\big)$ is related to the approximation of the Stratonovich integral, and that the expression of $\tilde{f}_j^{m+\frac{1}{2}}$ differs from that in Debussche & Di Menza (2002a,b) for two reasons. On one hand, we have a non-constant space mesh—this will be needed in

Section 4—and on the other hand, even if the space mesh Δx_j is constant (equal to Δx), the extra factor $\frac{\sqrt{3}}{2}$ comes from the fact that we have changed the basis $\{e_j\}_{0\le j\le N}$. For a constant space mesh h, we have

$$\tilde{f}_j^{m+\frac{1}{2}} = \frac{\sqrt{3}}{2}\frac{1}{\sqrt{\Delta t_m}\,\sqrt{\Delta x}}\chi_j^{m+\frac{1}{2}}, \quad j = 0, \cdots, N.$$

Next, denote $V_j^m = |u_j^m|^{2\sigma}$ and let $f_j^{m+\frac{1}{2}}$ be defined by (3.4), (3.6) and (3.7). Note that $\{\tilde{f}_j^m\}$ then define additive noise. At the half-time step, we let

$$u_j^{m+\frac{1}{2}} = \frac{1}{2}(u_j^m + u_j^{m+1}) \quad \text{and} \quad V_j^{m+\frac{1}{2}} = \left|u_j^{m+\frac{1}{2}}\right|^{2\sigma}.$$

To summarize, the discrete version of noise that we consider in this work is defined as follows:

$$g_j^{m+\frac{1}{2}} = \begin{cases} \epsilon f_j^{m+\frac{1}{2}}, & \text{multiplicative case,} \\ \epsilon \tilde{f}_j^{m+\frac{1}{2}}, & \text{additive case,} \end{cases} \tag{3.8}$$

where $\{f_j\}$s and $\{\tilde{f}_j\}$s are defined in (3.4), (3.6) and (3.7).

3.2 *Three schemes*

We now consider three schemes: the MEC scheme (also used in Debussche & Di Menza, 2002b)

$$i\frac{u_j^{m+1} - u_j^m}{\Delta t_m} + \mathcal{D}_2 u_j^{m+\frac{1}{2}} + \frac{1}{\sigma+1}\frac{|u_j^{m+1}|^{2(\sigma+1)} - |u_j^m|^{2(\sigma+1)}}{|u_j^{m+1}|^2 - |u_j^m|^2}u_j^{m+\frac{1}{2}} = g_j^{m+\frac{1}{2}}, \tag{3.9}$$

the CN scheme (which is a Taylor expansion of the previous one)

$$i\frac{u_j^{m+1} - u_j^m}{\Delta t_m} + \mathcal{D}_2 u_j^{m+\frac{1}{2}} + V_j^{m+\frac{1}{2}}u_j^{m+\frac{1}{2}} = g_j^{m+\frac{1}{2}} \tag{3.10}$$

and the new LE scheme, which uses the extrapolation of $V_j^{m+\frac{1}{2}}$

$$i\frac{u_j^{m+1} - u_j^m}{\Delta t_m} + \mathcal{D}_2 u_j^{m+\frac{1}{2}} + \frac{1}{2}\left(\frac{2\Delta t_{m-1} + \Delta t_m}{\Delta t_{m-1}}V_j^m - \frac{\Delta t_m}{\Delta t_{m-1}}V_j^{m-1}\right)u_j^{m+\frac{1}{2}} = g_j^{m+\frac{1}{2}}, \tag{3.11}$$

where $g_j^{m+\frac{1}{2}}$ is defined in (3.8).

To compare them, we note that the schemes (3.9) and (3.10) require to solve a nonlinear system at each time step, where the fixed point iteration or Newton iteration is involved (see Debussche & Di Menza, 2002b, for details). To implement the scheme (3.11), only a linear system needs to be solved at each time step. Numerically, these three schemes generate similar results (e.g. the discrete mass is conserved on the order of $10^{-10} - 10^{-12}$; see Fig. 1). The CN scheme (3.10) usually requires between

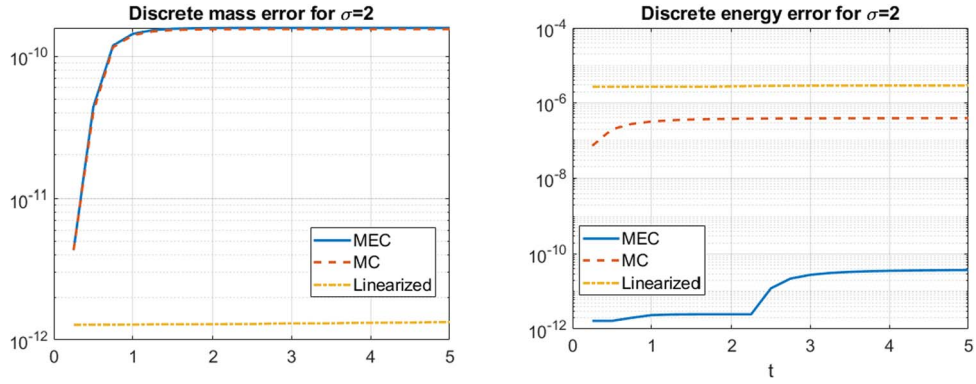

FIG. 1. Deterministic NLS ($\epsilon = 0$), L^2-critical case. Comparison of errors in the three schemes: MEC (3.9), CN (3.10) and LE (3.11). Left: error in mass computation. Right: error in energy computation.

2 and 8 iterations at each time step and thus, is about 3 times slower than the scheme (3.11), which requires no iteration. In its turn, the MEC scheme (3.9) is about 2–3 times slower than the CN (3.10). Thus, for the computational time, the last LE scheme (3.11) is the most convenient. We remark that the scheme (3.11) is a multi-step method. The first time step u^1 is obtained by applying either the scheme (3.10) or (3.9), and then we proceed with (3.11).

3.2.1 *Discrete mass and energy.* Let τ^*_{dis} denote the last (random) time the simulation is computed. We define the discrete mass by

$$M_{\text{dis}}[u^m] = \frac{1}{2}\sum_{j=0}^{N} |u_j^m|^2(\Delta x_j + \Delta x_{j-1}), \quad t_m \le \tau^*_{\text{dis}}. \tag{3.12}$$

For $m = 0$, it is the first-order approximation of the integral defining the mass $M(u_0)$ in (2.6).

We also define the discrete energy (similar to Debussche & Di Menza, 2002b), which is adapted to non-uniform mesh as follows for $t_m \le \tau^*_{\text{dis}}$

$$H_{\text{dis}}[u^m] := \frac{1}{2}\sum_{j=0}^{N} \frac{\left|u_{j+1}^m - u_j^m\right|^2}{\Delta x_j} - \frac{1}{2(\sigma+1)}\sum_{j=0}^{N} \frac{\left(\Delta x_j + \Delta x_{j-1}\right)}{2} |u_j^m|^{2(\sigma+1)}. \tag{3.13}$$

In order to check our numerical efficiency, we define the discrepancy of discrete mass and energy as

$$\mathcal{E}_1^m[M] := \max_m \left\{M_{\text{dis}}[u^m]\right\} - \min_m \left\{M_{\text{dis}}[u^m]\right\}. \tag{3.14}$$

And

$$\mathcal{E}^m[H] := \max_m \left\{H_{\text{dis}}[u^m]\right\} - \min_m \left\{H_{\text{dis}}[u^m]\right\}. \tag{3.15}$$

In the deterministic case, all three schemes conserve mass. In Fig. 1, we show that the LE scheme has the smallest error in discrete mass, since unlike the other two schemes there is no nonlinear system to solve, and thus, only the floating error comes into play. In the MEC and CN schemes, the error from solving the nonlinear systems accumulate at each time step. Consequently, the resulting error is accumulate slightly above (10^{-10}) (there, we take $|u^{m+1,k+1} - u^{m+1,k}| < 10^{-10}$ as the terminal condition for solving the nonlinear system in these two schemes, where k is the index of the fixed point iteration for computing $u^{m+1} = u^{m+1,\infty}$).

The MEC scheme (3.9) also conserves the discrete energy (3.13). While the other two schemes do not exactly conserve energy, the error of approximation is tolerable as shown on the right of Fig. 1. (Again, as we set up the tolerance $|u^{m+1,k+1} - u^{m+1,k}| < 10^{-10}$ in solving the resulting nonlinear system, the discrete energy error $\mathcal{E}^m[H]$ stays around 10^{-10}. Note that $\mathcal{E}^m[H]$ is a non-decreasing function in m; it increases slowly as time evolves.)

3.3 *Discrete mass and energy for a multiplicative noise*

We now consider a multiplicative noise or more precisely its discrete version as defined in (3.8). All three schemes conserve mass in this case.

LEMMA 3.1 The numerical schemes (3.9), (3.10) and (3.11) conserve the discrete mass, i.e. we have

$$M_{\text{dis}}[u^{m+1}] = M_{\text{dis}}[u^m], \quad m = 0, 1, \cdots, \quad t_{m+1} \le \tau^*_{\text{dis}}.$$

Proof. Multiply the equations (3.9), (3.10) or (3.11) by $\bar{u}_j^{m+\frac{1}{2}}(\Delta x_j + \Delta x_{j-1})$, sum among all indexes j, and take the imaginary part. Note that we impose the Neumann BC on both sides by setting the pseudo-points $u_{-1} = u_0$ and $u_N = u_{N+1}$. Then, with a straightforward computation, one obtains

$$M_{\text{dis}}[u^{m+1}] - M_{\text{dis}}[u^m] = 0,$$

which completes the proof. □

By Taylor's expansion, it is easy to see that the schemes (3.9) and (3.10) are of the second-order accuracy $O((\Delta t_m)^3)$ at each time step Δt_m. We say the scheme (3.11) is almost of the second-order accuracy because the residue is on the order $O((\Delta t_m)^2 \Delta t_{m-1})$. (Later, to make sure that blow-up solutions do not reach the blow-up time, we take the mth time step $\Delta t_m = \min\left\{\Delta t_{m-1}, \frac{\Delta t_0}{\|u^m\|^{2\sigma}_\infty}\right\}$. Thus, $\Delta t_m \le \Delta t_{m-1}$.) Therefore, while the schemes (3.10) and (3.9) seem to be slightly more accurate than (3.11), all three give the same order accuracy in their application below.

3.3.1 *Upper bounds on discrete energy.* We now study stability properties of the time evolution of the discrete energy (3.13) for the MEC scheme (3.9). Let τ^*_{dis} denote the random existence time of that scheme that is the last time the simulation is done. For simplicity, we take the uniform mesh in space and time, i.e. for each j and m, we set $\Delta x = \Delta x_j$ and $\Delta t = \Delta t_m$. In that case, the discrete energy is

$$H_{\text{dis}}[u^m] := \Delta x\Big(\frac{1}{2}\sum_{j=0}^{N}\Big|\frac{u^m_{j+1} - u^m_j}{\Delta x}\Big|^2 - \frac{1}{2(\sigma+1)}\sum_{j=0}^{N}|u^m_j|^{2(\sigma+1)}\Big).$$

PROPOSITION 3.2 Let $u_0 \in H^1$ and t_M be a point of the time grid. Then for $\Delta x \in (0,1)$

$$\mathbb{E}\big(1_{\{t_M \le \tau^*_{\rm dis}\}} H_{\rm dis}[u^M]\big) \le H_{\rm dis}[u^0] P(t_M \le \tau^*_{\rm dis}) + \frac{\epsilon\sqrt{3}}{2\sqrt{2}} \frac{\sqrt{\ln(2L_c) + |\ln(\Delta x)|}}{\sqrt{\Delta x}} \frac{1}{(\Delta t)^{\frac{3}{2}}} t_M, \tag{3.16}$$

$$\mathbb{E}\Big(1_{\{t_M \le \tau^*_{\rm dis}\}} \max_{0\le m\le M} H_{\rm dis}[u^m]\Big) \le H_{\rm dis}[u^0] P(t_M \le \tau^*_{\rm dis}) + \frac{\epsilon\sqrt{3}}{\sqrt{2}} \frac{\sqrt{\ln(2L_c) + |\ln(\Delta x)|}}{\sqrt{\Delta x}} \frac{1}{(\Delta t)^{\frac{3}{2}}} t_M. \tag{3.17}$$

Proof. Multiplying equation (3.9) by $-\Delta x\,(\bar{u}_j^{m+1} - \bar{u}_j^m)$, adding for $m = 0, ..., M-1$ and $j = 0, ..., N$, and using the conservation of the discrete energy in the deterministic case, we deduce that for some real-valued random variable $R(M,N)$, which changes from one line to the next, on the set $\{t_M \le \tau^*_{\rm dis}\}$

$$\begin{aligned} H_{\rm dis}[u^M] &= H_{\rm dis}[u^0] + iR(M,N) + \epsilon\,\Delta x \sum_{m=0}^{M-1}\sum_{j=0}^{N} (\bar{u}_j^{m+1} - \bar{u}_j^m)\,\frac{1}{2}\big(u_j^{m+1} + u_j^m\big)\tilde{f}_j^{m+\frac{1}{2}} \\ &= H_{\rm dis}[u^0] + iR(M,N) + \frac{\epsilon\,\Delta x}{2} \sum_{m=0}^{M-1}\sum_{j=0}^{N} \big(|u_j^{m+1}|^2 - |u_j^m|^2\big)\tilde{f}_j^{m+\frac{1}{2}}, \end{aligned} \tag{3.18}$$

$$= H_{\rm dis}[u^0] + iR(M,N) - \frac{\epsilon}{2}\frac{1}{\Delta t}\int_0^{t_M}\int_{\mathbb{R}} |U(s,x)|^2 W_N(\mathrm{d}s,\mathrm{d}x) + \frac{\epsilon\,\Delta x}{2}\sum_{m=0}^{M-1}\sum_{j=0}^{N} |u_j^{m+1}|^2 \tilde{f}_j^{m+\frac{1}{2}}, \tag{3.19}$$

where $U(s,x)$ is the step process defined by $U(s,x) = u_j^m$ on the rectangle $[t_m, t_{m+1}) \times [x_{j-\frac{1}{2}}, x_{j+\frac{1}{2}})$. Since the discrete mass is preserved by the scheme (Lemma 3.1), we have on the set $\{t_M \le \tau^*_{\rm dis}\}$

$$\frac{\epsilon\,\Delta x}{2}\sum_{m=0}^{M-1}\sum_{j=0}^{N} |u_j^{m+1}|^2 \tilde{f}_j^{m+\frac{1}{2}} \le \frac{\epsilon}{2}\sum_{m=0}^{M-1} \max_{0\le j\le N} |\tilde{f}_j^{m+\frac{1}{2}}| \sum_{j=0}^{N} \Delta x\,|u_j^{m+1}|^2 = \frac{\epsilon\,M_{\rm dis}[u^0]}{2}\sum_{m=0}^{M-1} \max_{0\le j\le N} |\tilde{f}_j^{m+\frac{1}{2}}|.$$

Using the definition of $\tilde{f}_j^{m+\frac{1}{2}}$ in (3.4), (3.6) and (3.7), we deduce

$$E\Big(\max_{0\le j\le N} |\tilde{f}_j^{m+\frac{1}{2}}|\Big) = \frac{\sqrt{3}}{2\sqrt{\Delta t}\sqrt{\Delta x}} E\Big(\max_{0\le j\le N} |\chi_j^{m+\frac{1}{2}}|\Big),$$

where the random variables $\chi_j^{m+\frac{1}{2}}$ are independent standard Gaussians.

Using Pisier's lemma (see e.g. Lifshits, 2012, Lemma 10.1), one observes that if $\{G_k\}_{k=1,...,n}$ are independent standard Gaussians and $M_n = \max_{1\le k\le n} |G_k|$, we have for $n \ge 2$

$$\mathbb{E}(M_n) \le \sqrt{2\,\ln(2\,n)}. \tag{3.20}$$

We enclose the proof below for the sake of completeness. For any $\lambda > 0$, using the Jensen inequality and the fact that $x \mapsto e^{\lambda x}$ is increasing, we deduce

$$\exp\Big(\lambda\,\mathbb{E}\Big[\max_{1\le k\le n}|G_k|\Big]\Big) \le \mathbb{E}\Big(\exp\Big[\lambda\max_{1\le k\le n}|G_k|\Big]\Big) \le \mathbb{E}\Big(\max_{1\le k\le n}\exp\big(\lambda|G_k|\big)\Big)$$
$$\le \sum_{k=1}^{n}\mathbb{E}\Big(e^{\lambda|G_k|}\Big) \le n\,2\,e^{\frac{\lambda^2}{2}}.$$

Taking logarithms, we obtain

$$\mathbb{E}\Big(\max_{1\le k\le n}|G_k|\Big) \le \frac{1}{\lambda}\ln\Big(2\,n\,e^{\frac{\lambda^2}{2}}\Big) = \frac{\ln(2\,n)}{\lambda} + \frac{\lambda}{2},$$

for every $\lambda > 0$. Choosing $\lambda = \sqrt{2\ln(2n)}$ concludes the proof of (3.20).

Keeping the real part of (3.19), we obtain

$$\mathbb{E}\big(1_{\{t_M\le\tau^*_{\rm dis}\}}\,H_{\rm dis}[u^M]\big) \le H_{\rm dis}[u^0]P(t_M \le \tau^*_{\rm dis}) + \frac{\epsilon}{2}M_{\rm dis}[u^0]\,M\,\frac{\sqrt{3}}{2}\sqrt{2\ln\big[2\,(N+1)\big]}\frac{1}{\sqrt{\Delta t}\sqrt{\Delta x}}$$
$$\le H_{\rm dis}[u^0]P(t_M \le \tau^*_{\rm dis}) + \frac{\epsilon\,\sqrt{3}}{2\,\sqrt{2}}\frac{1}{\sqrt{\Delta x}}\sqrt{\ln\Big(\frac{2\,L_c}{\Delta x}\Big)}\,\frac{1}{(\Delta t)^{\frac{3}{2}}}t_M.$$

This completes the proof of (3.16).

To prove (3.17), keeping the real part of (3.18) and estimating from above $|u_j^{m+1}|^2 - |u_j^m|^2$ by $|u_j^{m+1}|^2 + |u_j^m|^2$, we get on $\{t_M \le \tau^*_{\rm dis}\}$

$$\max_{0\le m\le M}H_{\rm dis}[u^M] = H_{\rm dis}[u^0] + \frac{\epsilon\,\Delta x}{2}\sum_{m=0}^{M-1}\sum_{j=0}^{N}\big(|u_j^{m+1}|^2 + |u_j^m|^2\big)\,|\tilde{f}_j^{\,m+\frac{1}{2}}|,$$

and the previous argument concludes the proof. □

REMARK 3.3 Note that in (3.18) and (3.19), the upper bound depends linearly on ϵ, and for small $\epsilon << 1$ so does the 'leading term' of the theoretical estimate (2.9). There is also a very small dependence on L_c, and a more important one on Δx and Δt. We remark that these are just the upper bounds, and to get a better idea about the growth and dependence of the energy on the various parameters, we investigate that numerically.

3.3.2 *Numerical tracking of discrete mass and energy.* Our analytical results above provide mass conservation and upper bounds on the expected values of energy. We would like to check numerically behaviour of these quantities. We start with testing the accuracy and efficiency of our schemes, for that we consider initial data $u_0 = A\,Q$, where $A > 0$ and Q is the ground state (1.4).

For the first test, we take $u_0 = 0.95Q$ and $\epsilon = 0.5$ in both L^2-critical ($\sigma = 2$) and L^2-supercritical ($\sigma = 3$) cases. The difference $\mathcal{E}_1^n$ in both cases is shown in Fig. 2 (left). Observe that the error is on the order of 10^{-15}, which is almost at the machine precision (10^{-16}).

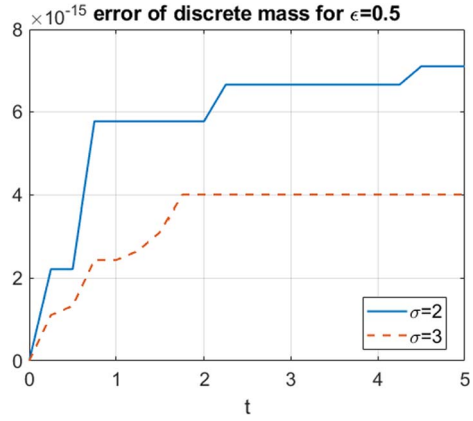

FIG. 2. Multiplicative noise. The error of the discrete mass computation $\mathcal{E}_1^m$ from (3.14), $\epsilon = 0.5$, in both L^2-critical and supercritical cases for one trajectory.

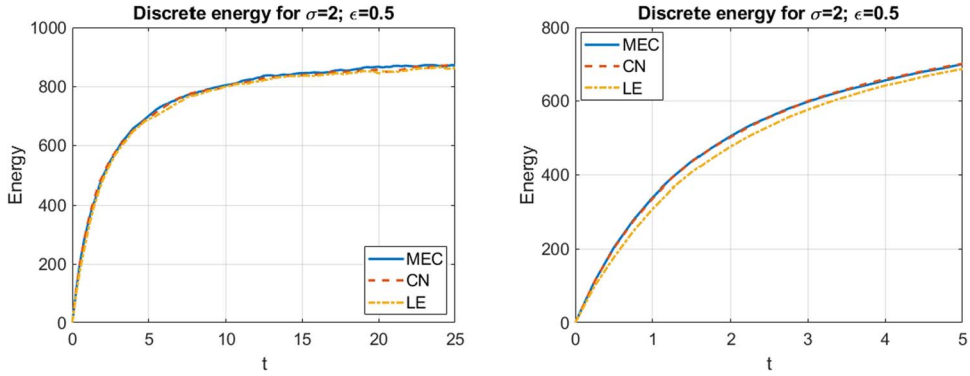

FIG. 3. Multiplicative noise, $\epsilon = 0.5$, L^2-critical case. Expected energy (averaged over 100 runs) using different schemes: MEC (3.9), CN (3.10) and LE (3.11). Left: time $0 < t < 25$. Right: zoom-in for time $0 < t < 5$: note only a small difference with the LE scheme.

Since not all of our three schemes conserve the discrete energy exactly (in the deterministic case), we study influence of the multiplicative noise onto the discrete energy (3.13). In Fig. 3, we show that in the L^2-critical case and $\epsilon = 0.5$, all three schemes produce the same result for the initial data $u_0 = 0.9Q$, where the energy is growing and then starts levelling off around the time $t = 15$. On the right of the same figure, we zoom on the time interval $[0, 5]$ to see better the difference between the schemes, and we note that the LE scheme produces slightly lower values of the energy, even if the overall behaviour is the same. In our further investigations, we usually use the MEC scheme if we need to track the mass and energy, and when we investigate the more global features such as blow-up profiles or run a lot of simulations, then we utilize the LE scheme.

We next study the growth of energy in time and the dependence on various parameters. In Figures 4, 6 and 7, we show the time dependence of solutions with initial data of type $u_0 = A\,Q$. In Fig. 4, we track the growth of the expected values of the instantaneous energy (on the left subplots) and of the supremum of energy (on the right subplots). To approximate the expected value, we average over 100 runs. Our

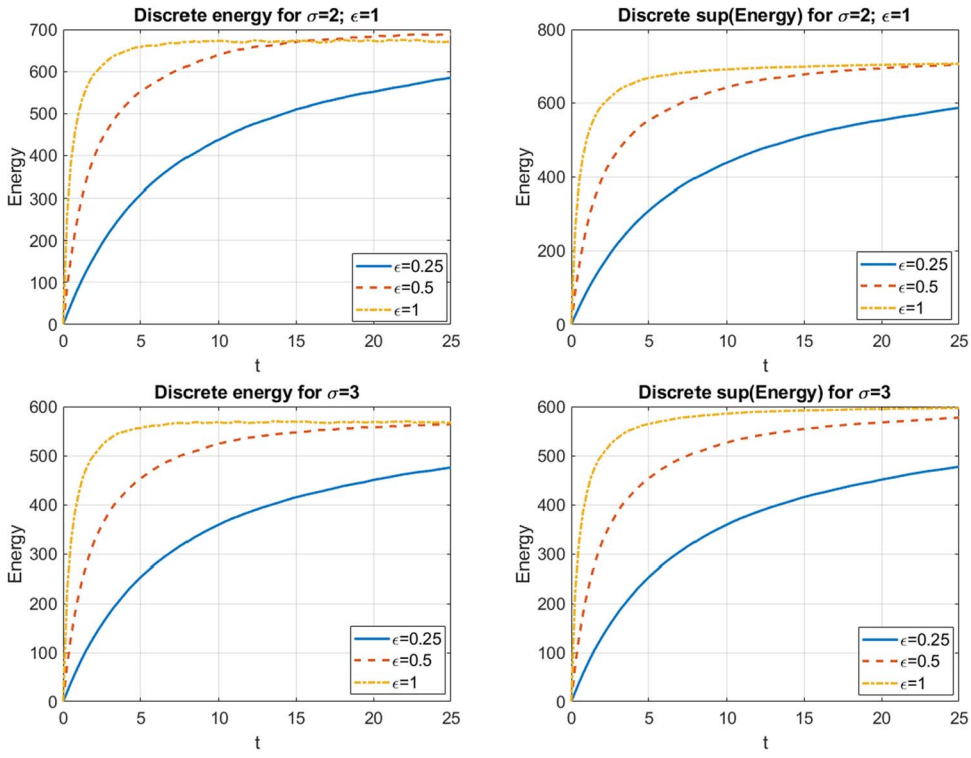

FIG. 4. Multiplicative noise in the L^2-critical case, $\sigma = 2$ (top) and L^2-supercritical case, $\sigma = 3$ (bottom); $u_0 = 0.8Q$, $\Delta x = 0.05$, $\Delta t = 0.005$, $L_c = 20$. Time dependence of $\mathbb{E}(H(u(t)))$ (left) vs. $\mathbb{E}(\sup_{s\le t} H(u(s)))$ (right) for various ϵ.

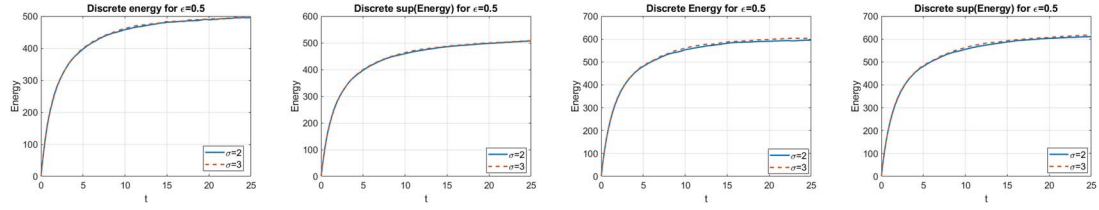

FIG. 5. Multiplicative noise in both L^2-critical and supercritical cases: gaussian (left two) $u_0 = e^{-x^2}$ and supergaussian (right two) $u_0 = e^{-x^4}$; $\Delta x = 0.05$, $\Delta t = 0.005$, $L_c = 20$. The time dependence of $\mathbb{E}(H(u(t)))$ (left) vs. $\mathbb{E}(\sup_{s\le t} H(u(s)))$ (right).

simulations show that both start growing linearly at first (see zoom-in Fig. 8), then start slowing down until they peak and level off to some possibly maximum value. As expected the values of the maximal energy up to some specific time are larger. We observe that the stronger the noise is (i.e. the larger the coefficient ϵ), the shorter it takes for the expected energy to start levelling off. A similar behaviour is seen in Fig. 5 for the gaussian initial data $u_0 = A\,e^{-x^2}$ and supergaussian data $u_0 = A\,e^{-x^4}$ in both critical and supercritical cases. From now on, we only show expectations of instantaneous energy in our figures as plots for the maximal energy are very similar.

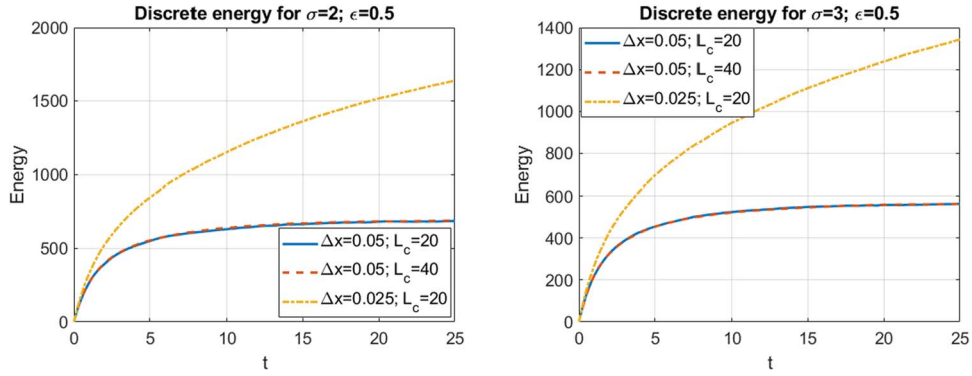

FIG. 6. Multiplicative noise, $u_0 = 0.8Q$, $\epsilon = 0.5$. The growth of expected energy depends on Δx but not on L_c in both L^2-critical (left) and supercritical (right) cases.

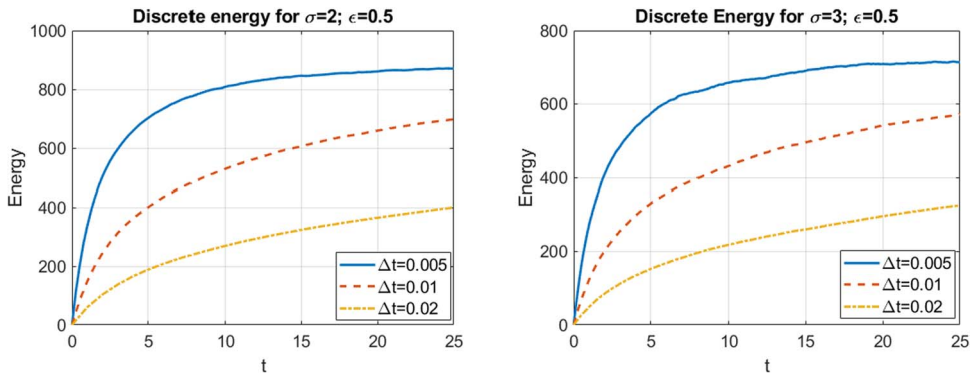

FIG. 7. Multiplicative noise, $u_0 = 0.9Q$, $\epsilon = 0.5$, $L_c = 20$, $\Delta x = 0.05$, $\Delta t = 0.005$. The growth of the expected energy for different Δt in both the L^2-critical and supercritical cases.

We next investigate the dependence of the discrete energy (3.13) on computational parameters such as the length of the interval L_c, the spatial step size Δx and the time step Δt. The results are shown in Fig. 6 for the expected energy values $\mathbb{E}(H(u(t)))$ with varying sizes of Δx and L_c; in Fig. 7, the dependence on Δt is displayed.

We remark that in both critical and supercritical cases, the computed values of expected energies (instantaneous and sup) are insensitive to the length of the computational domain L_c. However, there is a dependence on the mesh size Δx: the smaller step size results in a larger value of energy; there is also a dependence on the time step Δt.

3.4 *Discrete mass and energy for an additive noise*

Our next endeavor is to study the additive stochastic perturbation $f(u) = W(dt, \mathrm{d}x)$ or its discretized version in (3.8). As in the multiplicative case, we replace the space-time white noise W by its approximation W_N defined in (2.2) in terms of the functions $\{e_j\}_{0\le j\le N}$ described in (2.3). Then in

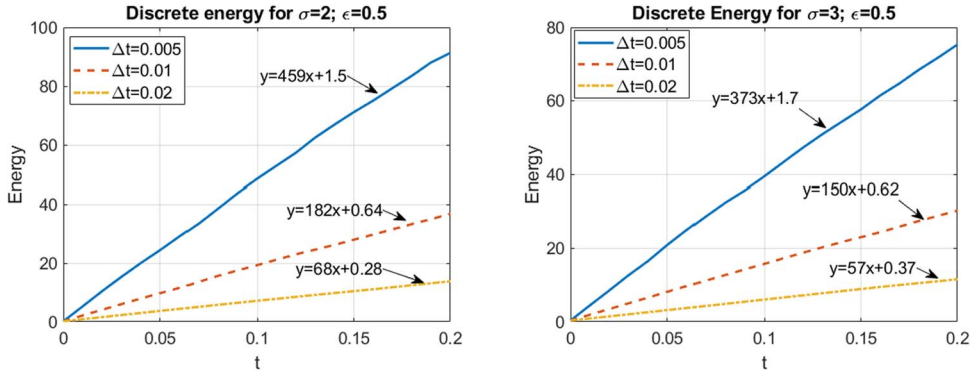

FIG. 8. Multiplicative noise. Zoom in for small times (to track linear dependence): $u_0 = 0.9Q$, $\Delta x = 0.05$, $L_c = 20$, $\epsilon = 0.5$. The time dependence of $\mathbb{E}(H(u(t)))$ for different values of Δt in both L^2-critical and supercritical cases.

our numerical schemes (3.9), (3.10) and (3.11) the right-hand side is $\left\{\tilde{f}_j^{m+\frac{1}{2}}\right\}$ defined in (3.5) for $j = 1, ..., N-1$, in (3.6) for $j = 0$, and in (3.7) for $j = N$.

We show that for the schemes (3.9), (3.10) and (3.11) the time evolution of the expected value of the discrete mass on the time interval $[0, T]$ is estimated from above by an affine function $a + bt$. We prove that the slope b is a linear function of the length L_c of the discretization interval $[-L_c, L_c]$. Therefore, our upper bounds on the discrete mass and energy depend linearly on the total length L_c ; they are inversely proportional to the constant time and space mesh sizes Δt and Δx. We do not claim that our upper bounds are sharp; this is the first attempt to upper estimate the discrete quantities.

3.4.1 *Upper bounds on discrete mass and energy with additive noise.* Recall that the discrete mass of u^m is defined by $M_{\text{dis}}[u^m] = \Delta x \sum_{j=0}^{N} |u_j^m|^2$. Let τ_{dis}^* be the maximal existence time of the discrete scheme (MEC) described in (3.9).

PROPOSITION 3.4 Let u_j^m be the solution to the scheme (3.9), (3.10) or (3.11) with $\tilde{f}_j^{m+\frac{1}{2}}$ instead of $f_j^{m+\frac{1}{2}}$ for a constant time mesh Δt and space mesh Δx.

Then given $T \geq 2\Delta t$ and any element $t_M \leq T$ of the time grid, we have

$$\mathbb{E}\big(1_{\{t_M \leq \tau_{\text{dis}}^*\}} M_{\text{dis}}[u^M]\big) \leq (1+\alpha) M_{\text{dis}}[u^0] + \frac{3T\,(1+\alpha)}{4\,\ln(1+\alpha)}\,\epsilon^2\,\frac{L_c}{\Delta x}\,\frac{t_M}{\Delta t}, \quad \alpha \in (0,1), \tag{3.21}$$

$$\mathbb{E}\Big(1_{\{t_M \leq \tau_{\text{dis}}^*\}} \max_{0 \leq m \leq M} M_{\text{dis}}[u^m]\Big) \leq \Big(1 + \alpha + \frac{\alpha}{2T}\Big) M_{\text{dis}}[u^0] + \frac{3\,T\,(1+\alpha)^2}{2\,\alpha}\,\epsilon^2\,\frac{L_c}{\Delta x}\,\frac{t_M}{\Delta t}, \ \alpha > 0. \tag{3.22}$$

Proof. Recall that $u_j^{m+\frac{1}{2}} = \frac{1}{2}\big(u_j^m + u_j^{m+1}\big)$. Multiply the equation (3.9) by $-2i\Delta t \Delta x\, \bar{u}_j^{m+\frac{1}{2}}$, sum on j from $j = 0$ to N and then sum on m from $m = 0$ to $M-1$ for $t_M \leq \tau_{\text{dis}}^*$. Then there exists a real-valued

random variable $R(M,N)$ (changing from one line to the next) such that on $\{t_M \le \tau^*_{\rm dis}\}$

$$\Delta x \sum_{j=0}^{N} |u_j^M|^2 - \Delta x \sum_{j=0}^{N} |u_j^0|^2 = iR(M,N) \; - 2\,\epsilon i \sum_{m=0}^{M-1}\sum_{j=0}^{N} \Delta t\,\Delta x\, \frac{\bar u_j^{\,m} + \bar u_j^{\,m+1}}{2}\, \tilde f_j^{\,m+\frac12}$$

$$= iR(M,N) \; - \epsilon \int_0^{t_M}\int_{\mathbb{R}} \mathrm{Im}\left(U(s,x)\right) W_N(\mathrm{d}s,\mathrm{d}x) - \epsilon \sum_{m=0}^{M-1}\sum_{j=0}^{N} \Delta t\,\Delta x\, \mathrm{Im}\,(u_j^{m+1})\tilde f_j^{\,m+\frac12}, \tag{3.23}$$

where U is the step process defined by $U(s,x) = u_j^m$ on the rectangle $[t_m, t_{m+1}) \times [x_{j-\frac12}, x_{j+\frac12})$. The Cauchy–Schwarz inequality applied to $\sum_m \sum_j$, the definition of $\tilde f_j^{\,m+\frac12}$ in (3.4), (3.6) and (3.7), and Young's inequality imply that for $\delta > 0$ we have

$$\Big|\epsilon \sum_{m=0}^{M-1}\sum_{j=0}^{N} \Delta t\,\Delta x\, \mathrm{Im}\,(u_j^{m+1})\tilde f_j^{\,m+\frac12}\Big| \le \epsilon \Big\{\sum_{m=1}^{M}\sum_{j=0}^{N} \Delta t\,\Delta x\, |u_j^m|^2\Big\}^{\frac12} \Big\{\sum_{m=0}^{M-1}\sum_{j=0}^{N} \Delta t\,\Delta x\, |\tilde f_j^{\,m+\frac12}|^2\Big\}^{\frac12}$$

$$\le \delta \sum_{m=1}^{M} \Delta t\, M_{\rm dis}[u^m] + \frac{3\,\epsilon^2}{16\,\delta} \sum_{m=0}^{M-1}\sum_{j=0}^{N} \frac34 |\chi_j^{\,m+\frac12}|^2, \tag{3.24}$$

where the random variables $\chi_j^{\,m+\frac12}$ are (as before) independent standard Gaussian random variables.

Keeping the real part in (3.23), then plugging the above estimate into the (3.23) and taking expected values (note that the process U is adapted), we deduce

$$\mathbb{E}\big(1_{\{t_M \le \tau^*_{\rm dis}\}}\, M_{\rm dis}[u^M]\big) \le M_{\rm dis}[u^0] + \frac{3\,\epsilon^2}{16\,\delta} M(N+1) + \delta \sum_{m=1}^{M} \Delta t \mathbb{E}\big(1_{\{t_M \le \tau^*_{\rm dis}\}}\, M_{\rm dis}[u^m]\big).$$

Given $\beta \in (0,1)$, we suppose that $\delta\,\Delta t \le \beta$. Then the discrete version of the Gronwall lemma (see e.g. Holte, 2009, Lemma 1) implies

$$\mathbb{E}\big(1_{\{t_M \le \tau^*_{\rm dis}\}}\, M_{\rm dis}[u^M]\big) \le \frac{1}{1-\beta}\Big[M_{\rm dis}[u^0] + \frac{3\,\epsilon^2}{16\,\delta} M(N+1)\Big] e^{\delta(M-1)\Delta t}.$$

Fix $\alpha \in (0,1)$ and choose $\beta \in (0,1)$ such that $\frac{1}{1-\beta} = \sqrt{1+\alpha}$, and choose $\delta > 0$ such that $e^{\delta T} = \sqrt{1+\alpha}$. Then $\delta = \frac{\ln(1+\alpha)}{2T} \in \big(\frac{\alpha}{4T}, \frac{\alpha}{2T}\big)$, and $\Delta t \le \frac{T}{1+\alpha} \le \frac{2T}{(\sqrt{1+\alpha}+1)\sqrt{1+\alpha}} = \frac{2T}{\alpha}\beta$ implies $\delta\,\Delta t \le \beta$. Furthermore, $M(N+1) \le \frac{t_M}{\Delta t}\frac{2L_c}{\Delta x}$, and we deduce (3.21).

We next prove (3.22). A similar computation, based on the first upper estimate in (3.23) and on (3.24), proves that for $\delta > 0$ we have on $\{t_M \leq \tau^*_{\rm dis}\}$

$$M_{\rm dis}[u^M] = M_{\rm dis}[u^0] + \epsilon \Big| \sum_{m=0}^{M-1} \sum_{j=0}^{N} \Delta t\, \Delta x\, {\rm Im}\,(u_j^m) \tilde{f}_j^{m+\frac{1}{2}} \Big| + \epsilon \sum_{m=0}^{M-1} \sum_{j=0}^{N} \Delta t\, \Delta x\, {\rm Im}\,(u_j^{m+1}) \tilde{f}_j^{m+\frac{1}{2}},$$

$$\leq M_{\rm dis}[u^0] + \delta \Delta t\, M_{\rm dis}[u^0] + 2\delta \sum_{m=1}^{M} \Delta t\, M_{\rm dis}[u^m] + 2 \frac{\epsilon^2}{4\,\delta} \sum_{m=0}^{M-1} \sum_{j=0}^{N} \frac{3}{4} |\chi_j^{m+\frac{1}{2}}|^2, \qquad (3.25)$$

where the random variables $\chi_j^{m+\frac{1}{2}}$ (as before) are independent standard Gaussian random variables. Taking expected values, we deduce for any $\delta > 0$

$$\mathbb{E}\Big(1_{\{t_M \leq \tau^*_{\rm dis}\}} \max_{1\leq m\leq M} M_{\rm dis}[u^m]\Big) \leq \quad (1 + \delta\Delta t) M_{\rm dis}[u^0] + 2\,\delta\, t_M\, \mathbb{E}\Big(1_{\{t_M \leq \tau^*_{\rm dis}\}} \max_{1\leq m\leq M} M_{\rm dis}[u^m]\Big)$$

$$+ \frac{3\,\epsilon^2}{8\,\delta}\, M\,(N+1).$$

Given $\beta > 0$, choose $\delta > 0$ such that $2\,\delta T = \beta$; this yields

$$\mathbb{E}\Big(\max_{1\leq m\leq M} 1_{\{t_M \leq \tau^*_{\rm dis}\}}\, M_{\rm dis}[u^m]\Big) \leq \frac{1}{1-\beta}\Big[\big(1 + \delta\Delta t\big) M_{\rm dis}[u^0] + \frac{3\,\epsilon^2}{8\,\delta}\, M\,(N+1)\Big].$$

Given $\alpha > 0$, choose $\beta \in (0,1)$ such that $\frac{1}{1-\beta} = 1 + \alpha$; then $\delta = \frac{\alpha}{2T(1+\alpha)}$. This concludes the proof of (3.22) for the MEC scheme.

A similar argument is applied to the schemes (3.10) and (3.11) (with the additive right-hand side); the only difference is in the real-valued random variable $R(M,N)$, which varies from one scheme to the next but is not present in the final estimate. □

REMARK 3.5 Note that the estimates (3.21) and (3.22) of the instantaneous and maximal mass are worse than the discrete analog of (2.11) by a factor of $\frac{1}{\Delta t}$. One might try to solve this problem in the proof, changing $2\bar{u}_j^{m+\frac{1}{2}} \tilde{f}_j^{m+\frac{1}{2}}$ into $\big(\bar{u}_j^{m+1} - \bar{u}_j^m\big) \tilde{f}_j^{m+\frac{1}{2}} + 2\,\bar{u}_j^m \tilde{f}_j^{m+\frac{1}{2}}$, and using again the scheme to deal with the first term. This would introduce an extra Δt factor. However, if the product of the two stochastic Gaussian variables would give a discrete analog of the inequality (2.11), the deterministic part of the scheme would still create terms involving $\bar{u}_j^{m+1} \tilde{f}_j^{m+\frac{1}{2}}$. The corresponding nonlinear 'potential' term would yield the mass to be raised to a large power to enable the use of the discrete Gronwall or Young lemma.

We next study stability properties of the time evolution of the discrete energy defined by (3.13) for the MEC scheme (3.9) in the additive case.

PROPOSITION 3.6 Let u_j^n be the solution to the scheme (3.9) with $\tilde{f}_j^{m+\frac{1}{2}}$ in (3.8) for a constant time mesh Δt and space mesh Δx. Then given $T \geq 2\Delta t$ and any element $t_M \leq T$ of the time grid, we have

$$\mathbb{E}\big(1_{\{t_M \leq \tau^*_{\rm dis}\}} H_{\rm dis}[u^M]\big) \leq (1+\alpha) H_{\rm dis}[u^0] P(t_M \leq \tau^*_{\rm dis}) + \frac{3T(1+\alpha)}{4\,\ln(1+\alpha)}\,\epsilon^2\,\frac{L_c}{\Delta x}\,\frac{t_M}{(\Delta t)^2},\ \alpha \in (0,1), \quad (3.26)$$

$$\mathbb{E}\Big(1_{\{t_M \leq \tau^*_{\rm dis}\}} \max_{0\leq m\leq M} H_{\rm dis}[u^m]\Big) \leq \Big(1+\alpha+\frac{\alpha}{2T}\Big) H_{\rm dis}[u^0] P(t_M \leq \tau^*_{\rm dis}) + \frac{3\,T\,(1+\alpha)^2}{2\,\alpha}\,\epsilon^2\,\frac{L_c}{\Delta x}\,\frac{t_M}{(\Delta t)^2},\ \alpha > 0. \quad (3.27)$$

Proof. Multiplying equation (3.9) by $-(\bar{u}_j^{m+1} - \bar{u}_j^m)\Delta x$, adding for $j = 0, ..., N$ and $m = 0, ..., M-1$ for $t_M \leq \tau^*_{\rm dis}$ and using the fact that in the deterministic case ($\epsilon = 0$) the scheme (3.9) preserves the discrete energy, we deduce the existence of a real-valued random variable $R(M,N)$ (changing from line to line) such that on $\{t_M \leq \tau^*_{\rm dis}\}$

$$\begin{aligned} H_{\rm dis}[u^M] =& H_{\rm dis}[u^0] + iR(M,N) - \epsilon\Delta x \sum_{m=0}^{M-1}\sum_{j=0}^{N} (\bar{u}_j^{m+1} - \bar{u}_j^m)\tilde{f}_j^{m+\frac{1}{2}} \\ =& H_{\rm dis}[u^0] + iR(M,N) + \epsilon\,\frac{\Delta x}{\Delta t}\int_0^{t_M} {\rm Re}\,(u_j^m)\,W_N({\rm d}s,{\rm d}x) - \epsilon\,\Delta x \sum_{m=0}^{M-1}\sum_{j=0}^{N} {\rm Re}\,u_j^{m+1}\,\tilde{f}_j^{m+\frac{1}{2}}. \end{aligned}$$

Notice that the last term in the above identity is similar to the last one in (3.23), except that the factor Δt is missing. Thus, the arguments used to prove Proposition 3.4 conclude the proof. □

3.4.2 *Numerical tracking of discrete mass and energy, additive noise.* As in the multiplicative case, we start with testing the accuracy of our three numerical schemes (3.9), (3.10) and (3.11) with the additive forcing (3.8) on the right-hand side and using the initial data $u_0 = A\,Q$. In Fig. 9, we show the comparison of three schemes for the initial condition $u_0 = 0.9Q$ with the strength of the noise $\epsilon = 0.05$ in the L^2-critical case. We see that for both discrete mass and energy the schemes behave similarly with very little variation from one to another.

We first investigate dependence of mass and energy on the strength of the noise ϵ. We take the initial condition $u_0 = 0.9\,Q$ and set $L_c = 20$, considering $x \in [-L_c, L_c]$; we also set $\Delta x = 0.05$ and $\Delta t = 0.005$. As before, we do 100 runs to approximate the expectation of either mass or energy. Recall that the identity (2.10) and the inequality (2.11) give linear dependence on time and square dependence on the noise strength ϵ, similar to that in our upper estimates for the discrete quantities (3.21) and (3.22) (for mass) and (3.26) and (3.27) (energy). The results are shown in Fig. 10, where we plot the expectation of the instantaneous quantities, $\mathbb{E}(M(u(t)))$ and $\mathbb{E}(H(u(t)))$. We omit figures for $\mathbb{E}(\sup_{s\leq t} M(u(s)))$ and $\mathbb{E}(\sup_{s\leq t} H(u(s)))$, since we get the same behaviour as shown in Fig. 10, and both discrete upper estimates (3.26) and (3.27) give similar dependence on all parameters.

Next, we show the dependence of the discrete mass and energy on the length of the computational interval L_c and the step size Δx. We compare the growth of both expected mass and energy for two values of the length $L_c = 20$ and $L_c = 40$, see Fig. 11, which shows the linear dependence for both

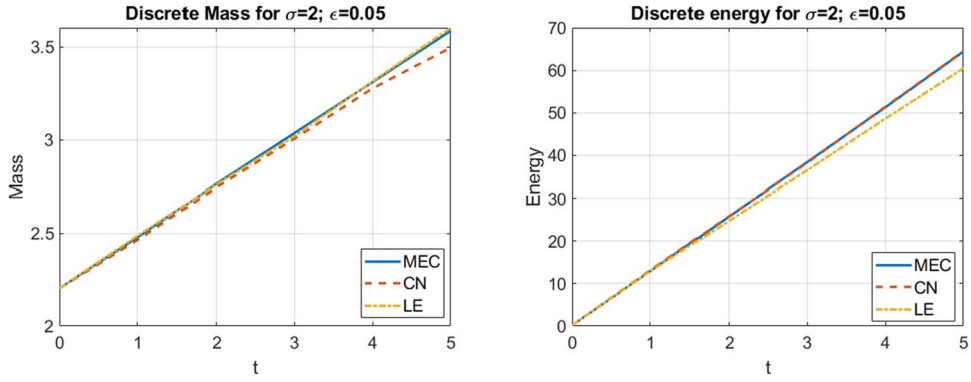

FIG. 9. Additive noise, $\epsilon = 0.05$, L^2-critical case. Time evolution of discrete mass (left) and energy (right) via different schemes: MEC (3.9), CN (3.10) and LE (3.11).

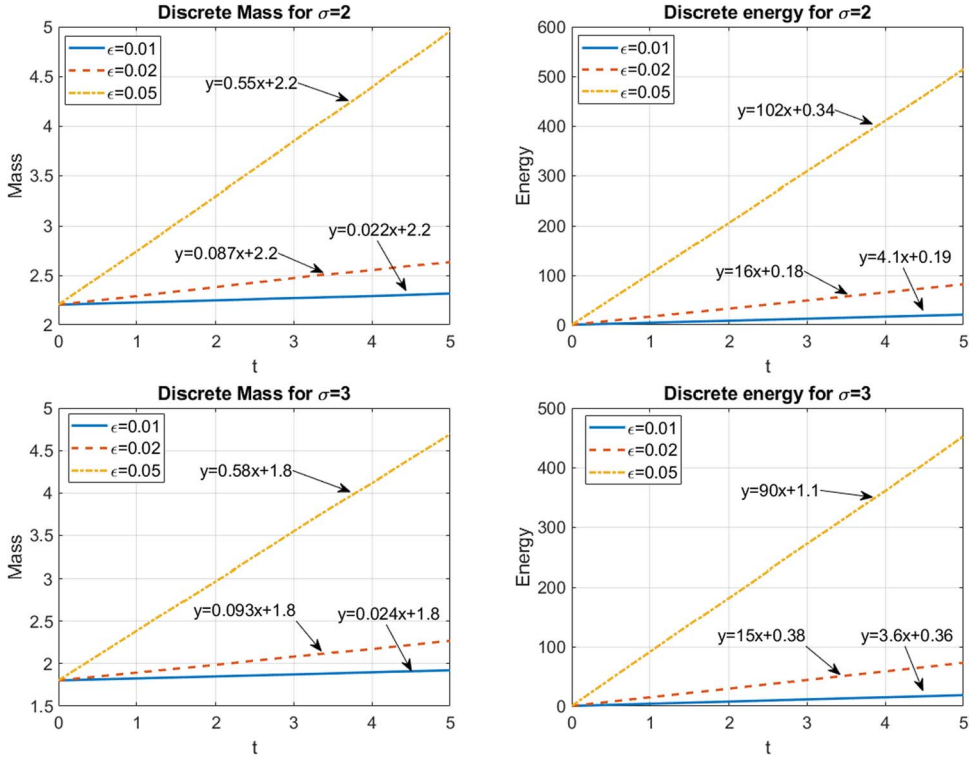

FIG. 10. Additive noise. Dependence of the expected value of (instantaneous) mass (left) and energy (right) on the strength of the noise ϵ. Top: L^2-critical ($\sigma = 2$), bottom: L^2-supercritical ($\sigma = 3$).

expected values of the mass and the energy: the L^2-critical case ($\sigma = 2$) is shown in the top row, and the L^2-supercritical case ($\sigma = 3$) is in the bottom row. Note that the slope doubles as we double the length of the computational interval L_c.

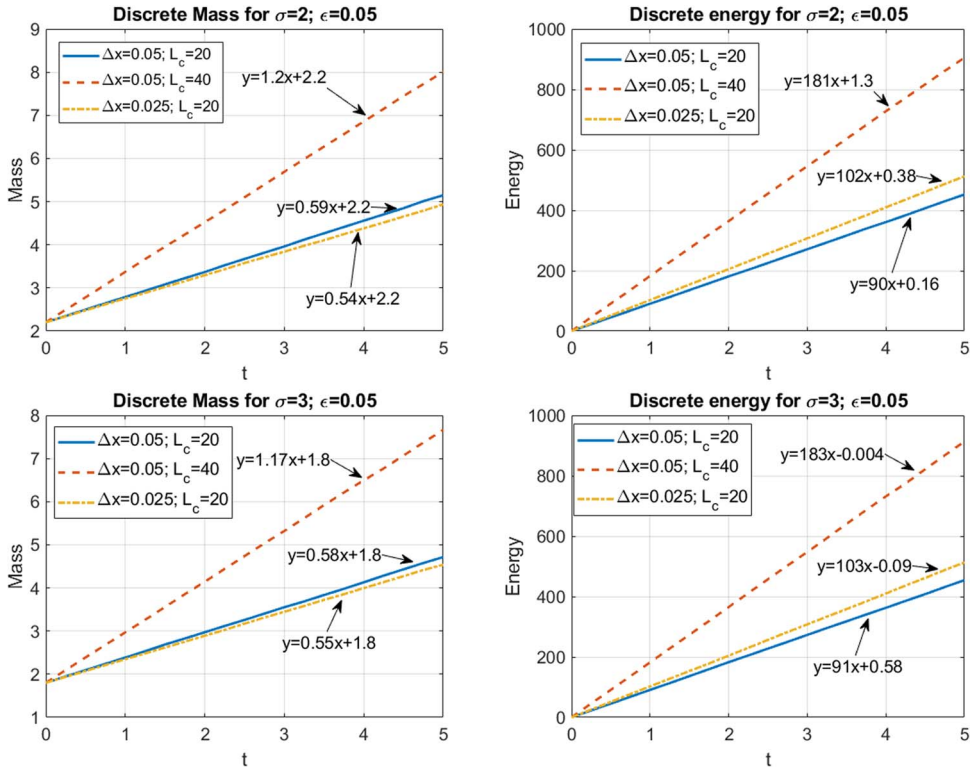

FIG. 11. Additive noise, $\epsilon = 0.05$. Dependence of the expected value of the mass and energy on the length of the interval L_c and space step-size Δx. Top: L^2-critical ($\sigma = 2$), bottom: L^2-supercritical ($\sigma = 3$).

The dependence on the time step-size of both discrete mass and energy is shown in Fig. 11. We show the dependence in the L^2-critical case and omit the supercritical case it is similar.

We also mention that we studied the growth of mass and energy for other initial data, e.g. gaussian $u_0 = A\, e^{-x^2}$, and obtained similar results, see Fig. 12.

In this section, we investigated how used-to-be conserved quantities (mass and energy) in the deterministic setting behave in the stochastic case with both multiplicative and additive approximations of the space-time white noise. Our next goal is to look at a global picture and study how behaviour of solutions is affected by the noise on a more global scale. We will see that in some cases the noise forces solutions to blow up and in other instances, the noise will prevent blow-up formation (similar investigations were done in Debussche & Di Menza (2002b) and references therein). We confirm some of their findings and then investigate the blow-up dynamics (rates, profiles, etc.). Before we venture into that study, we need to refine our numerical method, which we do in the next section.

4. Numerical approach, refined

To study solitons and their stability numerically, it is useful to have a 'non-uniform' mesh to appropriately capture certain spatial features. For that, we use a finite difference method with

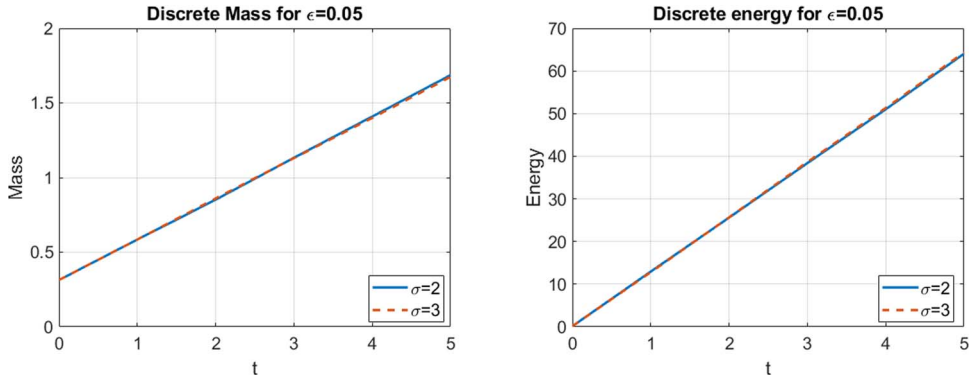

FIG. 12. Additive noise, $\epsilon = 0.05$. Time dependence of the discrete mass (left) and energy (right) for the gaussian initial condition $u_0 = 0.5\, e^{-x^2}$. (Here, both mass and energy coincide regardless of the nonlinearity, $\sigma = 2$ or 3, since the only dependence is in the potential part of energy, which creates a very small difference.)

non-uniform mesh. To study specific details of the evolution (such as formation of blow up), we implement a mesh refinement. We note that to keep our algorithm efficient, the mesh refinement is applied only at certain time steps, i.e. when it is necessary. The mesh-refinement process terminates when we stop the simulation, usually at the level $\|u\|_{L^\infty}^{\sigma} \sim 10^{12}$. By a carefully chosen mesh-refinement strategy and a specific interpolation during the refinement (which we introduce below), we are able to preserve the discrete mass at the same value before and after the mesh refinement. Thus, the discrete mass is exactly conserved at all times in our time evolution on $[0, T]$ (in the deterministic and multiplicative noise settings).

We note that in the deterministic theory, solutions either exist globally in time or blow up in finite time, and there are various results identifying thresholds for such a dichotomy. In the probabilistic setting, blow up may hold in finite time with some (positive) probability even for small initial data. Indeed in de Bouard & Debussche (2005), it is shown that for a multiplicative stochastic perturbation (driven by non-degenerate noise with a regular enough space correlation) given any non-null initial data there are blow up with positive probability. Therefore, when we study solutions of SNLS (1.1), we may refer to the types of solutions as globally existing (a.s.), long-time existing (perhaps with some estimates on the time of existence) and blow up in finite time (with positive probability, or a.s.) solutions.

We also mention that as an extra bonus for a multiplicative boise, our algorithm has very small fluctuation (on the order of 10^{-12}) in the difference of the actual mass (2.6), which is approximated by the composite trapezoid rule; see (4.11). The tiny difference is observed in all scenarios of solutions: globally existing, long-time existing and blow up in finite time (the difference is on the order of 10^{-12}), which we demonstrate in Fig. 2. This suggests that our algorithm is very accurate in all scenarios of solutions.

4.1 *Mesh-refinement strategy*

When a solution starts concentrating or localizing spatially, in order to increase accuracy, it is necessary to put more points into that region. For example, as blow up starts focusing towards a singular point as $t \to T$, the singular region will benefit from having more grid points. In this subsection, we discuss the mesh-refinement strategy. The idea comes from the scaling invariance of the NLS equation or the

dynamic rescaling method from LeMesurier *et al.* (1987), Sulem & Sulem (1999), Yang *et al.* (2018) and Yang *et al.* (2019).

At time 0, the computational interval $[-L_c, L_c]$ is discretized into $N_0 + 1$ grid points $\{x_0^0, \cdots, x_{N_0}^0\}$ (which may be equi-distributed, since we typically begin with a uniform space mesh). When we proceed, we check at each time step if the scheme fulfils a tolerance criterion, described below.

As we mentioned in the introduction, the stable blow-up dynamics for the deterministic NLS consists of the self-similar regime with the rescaled parameters

$$u(t,x) = \frac{1}{L(t)^{1/\sigma}} v(\tau, \xi), \quad \xi = \frac{x}{L(t)}, \quad \tau = \int_0^t \frac{1}{L^2(s)}\, \mathrm{d}s, \tag{4.1}$$

where $v(\xi, \tau)$ is a globally (in τ) defined self-similar solution. We do not rescale the equation (1.1) into a new equation as we do not use the dynamic rescaling method due to regularity issues. However, we still adopt the rescaling idea for our mesh-refinement algorithm. Assume ξ is equi-distributed for all time steps t_m and $\Delta\xi = \xi_1 - \xi_0$. Thus, we assume that there is a mapping $L(t_m)$, which maps the point $x_j^m \to \xi_j$. Using (4.1) or $L(t)^{1/\sigma} u(t) = v(\tau)$ with our discretization, we get

$$L(t_m)^{1/\sigma} \left(u(x_j^m) - u(x_{j-1}^m)\right) = v(\xi_j) - v(\xi_{j-1}), \tag{4.2}$$

where both sides are well behaved (since v is now global) and thus should have $O(1)$ value (referred to as the 'moderate' value) for $j = 0, 1, \cdots, N_m$. (The rescaled solution $v(\xi)$ is well behaved as well). Using the second relation in (4.1), we define the discretization of the mapping of $L(t_m)$ at each interval $[\xi_{j-1}, \xi_j]$:

$$L_j^m = \frac{x_j^m - x_{j-1}^m}{\Delta\xi}.$$

Putting this into (4.2) and using the fact that $\Delta\xi$ is a constant, we obtain that

$$C_d := \{x_j^m - x_{j-1}^m\}^{1/\sigma} \left(u(x_j^m) - u(x_{j-1}^m)\right)$$

remains 'moderate' as time evolves for each $j = 1, 2, \cdots, N_m$.

Therefore, we set the tolerance to be

$$M_{tol}^1 = Tol_1 \cdot \max_j \{(\Delta x_j^0)^{1/\sigma} \cdot |u_{j+1}^0 - u_j^0|\}, \tag{4.3}$$

where Tol_1 is the constant we choose at $t = t_0$ (e.g. $Tol_1 = 2, 2.5$ or 5). This criterion is focused on the size of the quantity $u_{j+1}^m - u_j^m$. As the solution reaches higher and higher amplitudes, we refine the grid and insert more points, in particular, to avoid the under-resolution issue.

In a similar way, we set

$$M_{tol}^2 = Tol_2 \cdot \max_j \{(\Delta x_j^0)^{1/\sigma} \cdot |u_{j+1}^0 + u_j^0|\}, \tag{4.4}$$

where Tol_2 is the constant we choose at the initial time $t = t_0$ (e.g. $Tol_2 = 0.5$ or 1).

At each time step t_m, we compute the quantities $\gamma_j^m = (\Delta x_j^m)^{1/\sigma} \cdot |u_{j+1}^m - u_j^m|$ and $\eta_j^m = (\Delta x_j^m)^{1/\sigma} \cdot |u_{j+1}^m + u_j^m|$ on each interval $[x_j^m, x_{j+1}^m]$. If at time $t = t_m$ we have $\gamma_j^m > M_{tol}^1$, or $\eta_j^m > M_{tol}^2$ for some j's, we divide the jth interval $[x_j^m, x_{j+1}^m]$ into two sub-intervals $[x_j^m, x_{j+\frac{1}{2}}^m]$ and $[x_{j+\frac{1}{2}}^m, x_{j+1}^m]$. Then, the new value $u_{j+\frac{1}{2}}^m$ is needed. We discuss the strategy for obtaining $u_{j+\frac{1}{2}}^m$ with the mass-preserving property in the next subsection. After using this midpoint refinement, we continue our time evolution to the next time step t_{m+1}. The mesh will be refined again if $\gamma_j^{\tilde{m}} > M_{tol}^1$ or $\eta_j^{\tilde{m}} > M_{tol}^2$ at some time $t = t_{\tilde{m}} > t_m$, i.e. the mesh-refinement process will be repeated until we terminate our simulation.

4.2 *Mass-conservative interpolation in the refinement*

Recall that when the tolerance is not satisfied at the jth interval, we refine the mesh by dividing that interval into two sub-intervals, and hence, we need an interpolation to find the new value of $u_{j+\frac{1}{2}}^m$ at the point $x_{j+\frac{1}{2}}^m = \frac{1}{2}(x_j^m + x_{j+1}^m)$.

A classical approach is to apply a linear interpolation (as, e.g. in Debussche & Di Menza, 2002b):

$$u_{j+\frac{1}{2}}^m = \frac{1}{2}(u_j^m + u_{j+1}^m).$$

When we add this middle point, the length of each interval $[x_j^m, x_{j+\frac{1}{2}}^m]$ and $[x_{j+\frac{1}{2}}^m, x_{j+1}^m]$ simply becomes $\frac{1}{2}\Delta x_j^m$. Unfortunately, this widely used linear interpolation does not conserve the discrete mass. Indeed, let the discrete mass at the jth interval before the mesh refinement be

$$M_j = \frac{1}{4}\big[|u_j^m|^2(\Delta x_j^m + \Delta x_{j-1}^m) + |u_{j+1}^m|^2(\Delta x_{j+1}^m + \Delta x_j^m)\big], \tag{4.5}$$

and the mass after the mesh refinement be defined as

$$\tilde{M}_j = \frac{1}{4}\left[|u_j^m|^2\Big(\frac{1}{2}\Delta x_j^m + \Delta x_{j-1}^m\Big) + |u_{j+\frac{1}{2}}^m|^2\Delta x_j^m + |u_{j+1}^m|^2\Big(\frac{1}{2}\Delta x_j^m + \Delta x_{j+1}^m\Big)\right]. \tag{4.6}$$

Then a simple computation shows that

$$M_j - \tilde{M}_j = \frac{1}{4}|u_j^m - u_{j+1}^m|^2\Delta x_j^m. \tag{4.7}$$

Hence, $\tilde{M}_j < M_j$ on some subset of Ω (where the random variables u_j^m and u_{j+1}^m differ), which is a non-empty set. In this linear interpolation, we suffer a loss of mass at each step of the mesh-refinement procedure. In another popular interpolation, via the cubic splines, a similar analysis shows that the scheme suffers the increase of mass at each step of the mesh-refinement procedure. To avoid these two problems, we proceed as follows.

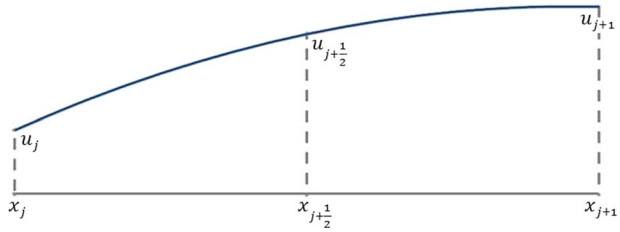

FIG. 13. Quadratic interpolation in (4.8) to obtain $u^m_{j+\frac{1}{2}}$ (index m is omitted).

We set the two quantities (4.5) and (4.6) to be equal to each other, i.e. $M_j = \tilde{M}_j$, by solving this equation with the fact that $x^m_{j+1} - x^m_{j+\frac{1}{2}} = x^m_{j+\frac{1}{2}} - x^m_j = \frac{1}{2}\Delta x^m_j$, we obtain

$$|u^m_{j+\frac{1}{2}}|^2 = \frac{1}{2}\left(|u^m_j|^2 + |u^m_{j+1}|^2\right). \tag{4.8}$$

To implement the condition (4.8), one choice is to set

$$\begin{cases} \mathrm{Re}(u^m_{j+\frac{1}{2}}) = \sqrt{\frac{1}{2}\left[\mathrm{Re}(u^m_j)^2 + \mathrm{Re}(u^m_{j+1})^2\right]}\,\mathrm{sgn}\big(\mathrm{Re}(u^m_j) + \mathrm{Re}(u^m_{j+1})\big), \\ \mathrm{Im}(u^m_{j+\frac{1}{2}}) = \sqrt{\frac{1}{2}\left[\mathrm{Im}(u^m_j)^2 + \mathrm{Im}(u^m_{j+1})^2\right]}\,\mathrm{sgn}\big(\mathrm{Im}(u^m_j) + \mathrm{Im}(u^m_{j+1})\big). \end{cases} \tag{4.9}$$

This is what we use in our simulations. We next describe the steps of our full numerical algorithm.

4.3 *The algorithm*

The full implementation of our algorithm proceeds as follows:

1. Discretize the space in the uniform mesh and set up the values of tolerance Tol_1 and Tol_2.
2. Apply the mass-conservative numerical schemes (3.9), (3.10) or (3.11) for the time evolution from u^{m-1} to reach u^m with the time step size Δt_{m-1}.
3. At $t = t_m$, change the time step size by $\Delta t_m = \frac{\Delta t_0}{\|u(\cdot,t_m)\|^{2\sigma}_\infty}$ for the next time evolution (thus, t never reaches the blow-up time T, in case there is a blow up).
4. If the solution meets the tolerance (Tol_1 or Tol_2) on some intervals $[x_j, x_{j+1}]$, we divide those intervals into two sub-intervals.
5. Apply the 'mass-conservative interpolation' (4.8) to obtain the value of $u^m_{j+\frac{1}{2}}$.
6. Continue with the time evolution to $t = t_{m+1}$ by applying (3.9), (3.10) or (3.11).
7. Repeat Steps 4 and 5 until the simulation is terminated.

A few remarks are due. First of all, this algorithm is applicable in the deterministic case. To our best knowledge, this is the first mesh-refinement numerical algorithm that 'conserves' the discrete mass exactly before and after the refinement, which is especially important when simulating the finite time

blow up in the 1D focusing nonlinear Schrödinger equation with or without stochastic perturbation. Moreover, in the deterministic and multiplicative noise cases, the discrete mass is conserved from the initial to terminal times. We note that in studying and simulating the blow-up solutions in the (deterministic) NLS equation, the dynamic rescaling or moving mesh methods are used (since solutions have some regularity); however, in the stochastic setting, those methods are simply not applicable because noise destroys regularity in the space variable.

Secondly, its full implementation is needed for solutions that concentrate locally or blow up in finite time, where the refinement and mass conservation are crucial features to ensure the reliability of the results. However, the algorithm is also applicable in the cases where the solution exists globally or long enough for numerical simulations. Indeed, if we start with the uniform mesh and remove the steps (1), (3), (4) and (5), it becomes a widely used second order numerical scheme for studying the NLS equation (in both deterministic and stochastic cases) without considering the singular solutions.

When investigating solutions, which do not form singularities (exist globally in time or on sufficiently long time interval), the procedures (1), (3), (4) and (5) are not necessary and we omit them. When studying the blow-up solutions (in Section 6), we incorporate fully all steps in order to obtain satisfactory results. When testing our simulations of blow-up solutions, not only the error of the discrete mass $\mathcal{E}_1^m[M]$ from (3.14) is checked but also the discrepancy of the actual mass, approximated by the composite trapezoid rule at each time step, is checked, i.e.

$$\mathcal{E}_2^m[M] = \max_m \left\{ M_{\text{app}}[u^m] \right\} - \min_m \left\{ M_{\text{app}}[u^m] \right\}, \tag{4.10}$$

where

$$M_{\text{app}}[u^m] = \frac{1}{2}|u_0^m|^2 \Delta x_0 + \sum_{j=1}^{N-2} |u_j^m| \Delta x_j + \frac{1}{2}|u_N^m|^2 \Delta x_{N-1}. \tag{4.11}$$

For this test, we choose $u_0 = 1.05Q$ and consider only the L^2-critical case ($\sigma = 2$), comparing $\epsilon = 0$ (deterministic case) with $\epsilon = 0.1$ (multiplicative noise case). The initial spatial step size is set to $\Delta x = 0.01$, and the initial temporal step-size is set to $\Delta t_0 = \Delta x/4$. We take the computational domain to be $[-L_c, L_c]$ with $L_c = 5$. Figure 14 shows the dependence of $\mathcal{E}_1^m$ and $\mathcal{E}_2^m$ on the focusing scaling parameter $L(t) = \frac{1}{\|u(t)\|_\infty^\sigma}$.

Observe that both the discrete mass and approximation of the actual mass are conserved well even when the focusing parameter reaches $\sim 10^{-12}$. Such high precision in mass conservation justifies well the efficiency of our schemes. We also tested other types of initial data (e.g. gaussian data $u_0 = A\, e^{-x^2}$), different noise strength ($\epsilon = 0.2, 0.5$) and the supercritical power of nonlinearity ($\sigma = 3$); the precision is similar to that shown in Fig. 14.

In the next two sections, we discuss global behaviour of solutions, showing how solitons behave for various nonlinearities (Section 5), and then investigate the formation of blow up (Section 6) including our findings on profiles, rates and localization.

5. Numerical simulations of global behaviour of solutions

We again consider initial data of type $u_0 = A\, Q$, where $A > 0$ and Q is the ground state (1.4). In the deterministic setting, one would consider two cases for numerical simulations, namely, $A < 1$ (which

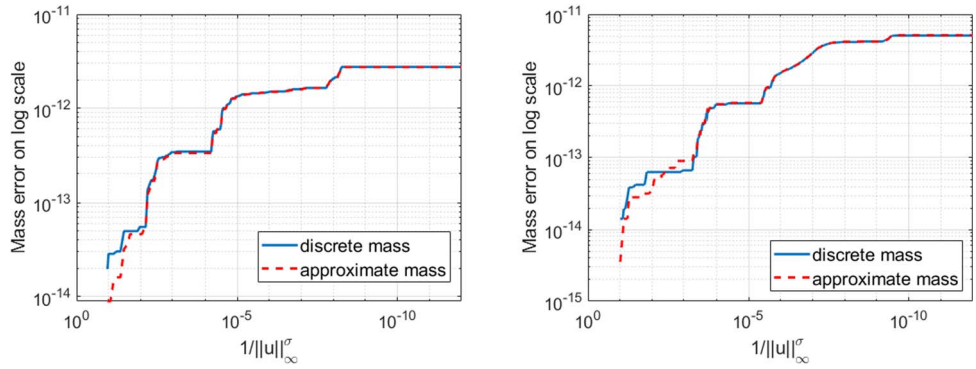

FIG. 14. The error of discrete and actual masses $\mathcal{E}_1^m$ and $\mathcal{E}_2^m$ for the L^2-critical case with or without the multiplicative noise. Left: $\epsilon = 0$ (deterministic case). Right: $\epsilon = 0.1$.

TABLE 1 *Additive noise. Percentage of blow-up solutions with initial data $u_0 = AQ$ in the L^2-critical case ($\sigma = 2$) with $N_t = 1000$ trials and running time $0 < t < 5$*

A	0.95	1	1.05
$\epsilon = 0.01$	0	0.34	1
$\epsilon = 0.05$	0.028	0.926	1
$\epsilon = 0.1$	0.984	0.999	0.999

TABLE 2 *Additive noise. Percentage of blow-up solutions with initial data $u_0 = AQ$ in the L^2-supercritical case ($\sigma = 3$) with $N_t = 1000$ trials and running time $0 < t < 5$*

A	0.95	1	1.05
$\epsilon = 0.01$	0	0.753	1
$\epsilon = 0.05$	0.030	0.983	1
$\epsilon = 0.1$	0.986	1	1

guarantees the global existence and $A > 1$ (which could be used to study blow-up solutions). In the stochastic setting, we use similar data; however, as we will see (in Table 1), we may not know *a priori* if the solution is global or blows up in finite time (a.s. or with some positive probability). For example, the condition $A < 1$ does not necessarily guarantee global existence or even sufficiently long (for numerical simulations) time existence as can be seen in Tables 1 and 2.

We consider additive noise first. Putting sufficiently large ϵ and tracking for a sufficiently long time, we observe that small data leads to blow up for the cases $\sigma = 2$ and $\sigma = 3$. For example, in Fig. 15, we take $u_0 = 0.5Q$ (far below the deterministic threshold) with sufficiently strong noise $\epsilon = 0.1$ and run for (computationally) long time: the fixed point iteration for solving the MEC scheme (3.9) fails to converge after 2000 iterations at time $t \approx 19.485$, which indicates that u^{m+1} is far from u^m at $t_m \approx 19.485$. The numerical scheme cannot be run any further, and this is typically considered as the indication of the blow-up formation (see below comparison with the L^2-subcritical case).

Figure 15 shows that the additive noise can 'create' blow up in finite time. In other words, the initial data, which in the deterministic case were to produce a globally existing scattering solution, in the additive forcing case could evolve towards the blow up. This is partially due to the fact that the additive

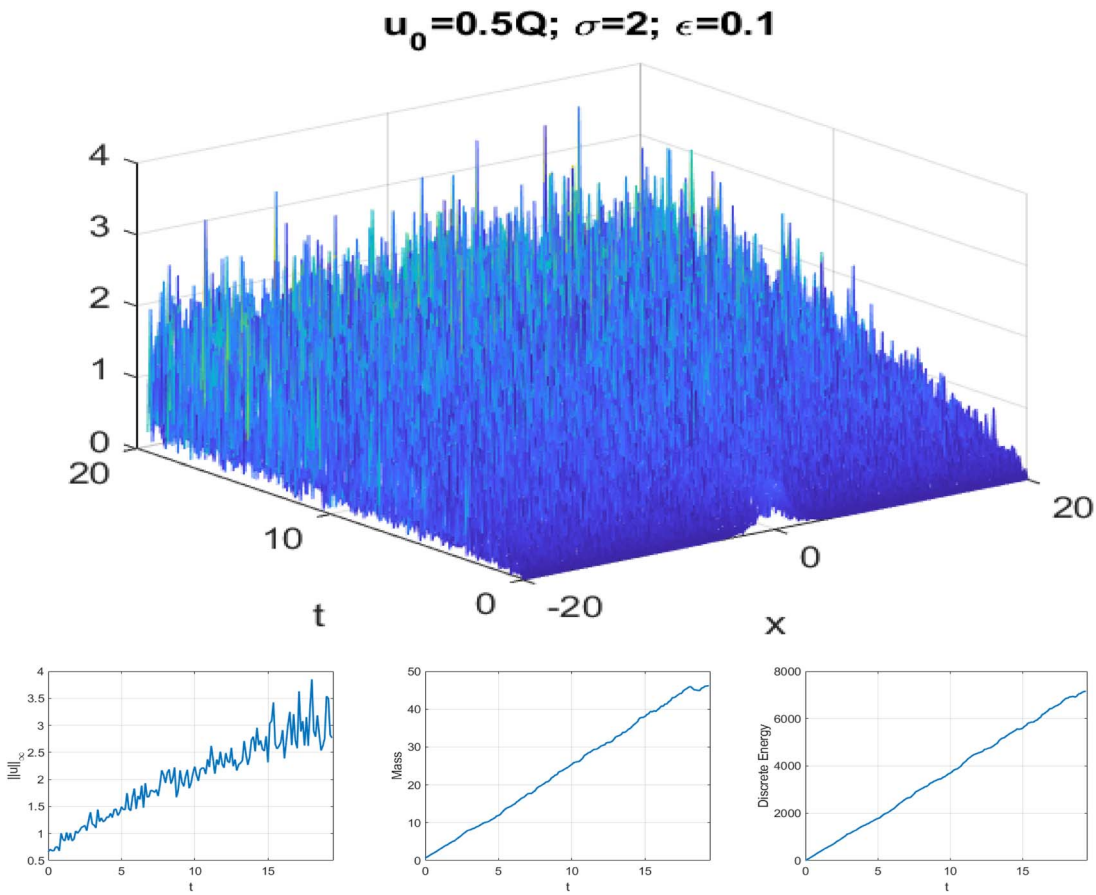

FIG. 15. Additive noise, $\epsilon = 0.1$, $u_0 = 0.5Q$, L^2-critical case. The solution grows in time until the fixed point iteration fails. Bottom: time dependence of $\|u\|_\infty$, mass and energy.

noise makes the mass and energy grow in time; see the bottom subplots in Fig. 15, where both mass and energy grow linearly in time. Note that we start with a single soliton profile with a small amplitude ($0.5\,Q$) and eventually the noise destroys the soliton profile with the growing L^∞ norm (left bottom subplot in Fig. 15).

It is also interesting to compare this behaviour with the L^2-subcritical case ($\sigma = 1$), where in the deterministic case all solutions are global (there is no blow up for any data), see de Bouard & Debussche (2003). Figure 16 shows time evolution of the initial condition $u_0 = 1.5Q$ with the strength of the additive noise $\epsilon = 0.1$ (same as in Fig. 15). While the soliton profile is distinct for the time of the computation, it is obviously getting corrupted by noise: the L^∞ norm is slowly increasing with some wild oscillations. One can also observe that mass and energy grow linearly to infinity (as $t \to \infty$); see bottom plots of Fig. 16. Note that while there is growth of mass and energy, as well as the L^∞ norm in this subcritical case, the fixed point iteration does not fail, indicating that there is no blow up.

For comparison, we also show the influence of smaller noise $\epsilon = 0.05$ on a larger time scale ($0 < t < 50$) for the initial condition $u_0 = Q$; see Fig. 17. The smaller noise also seems to destroy the soliton

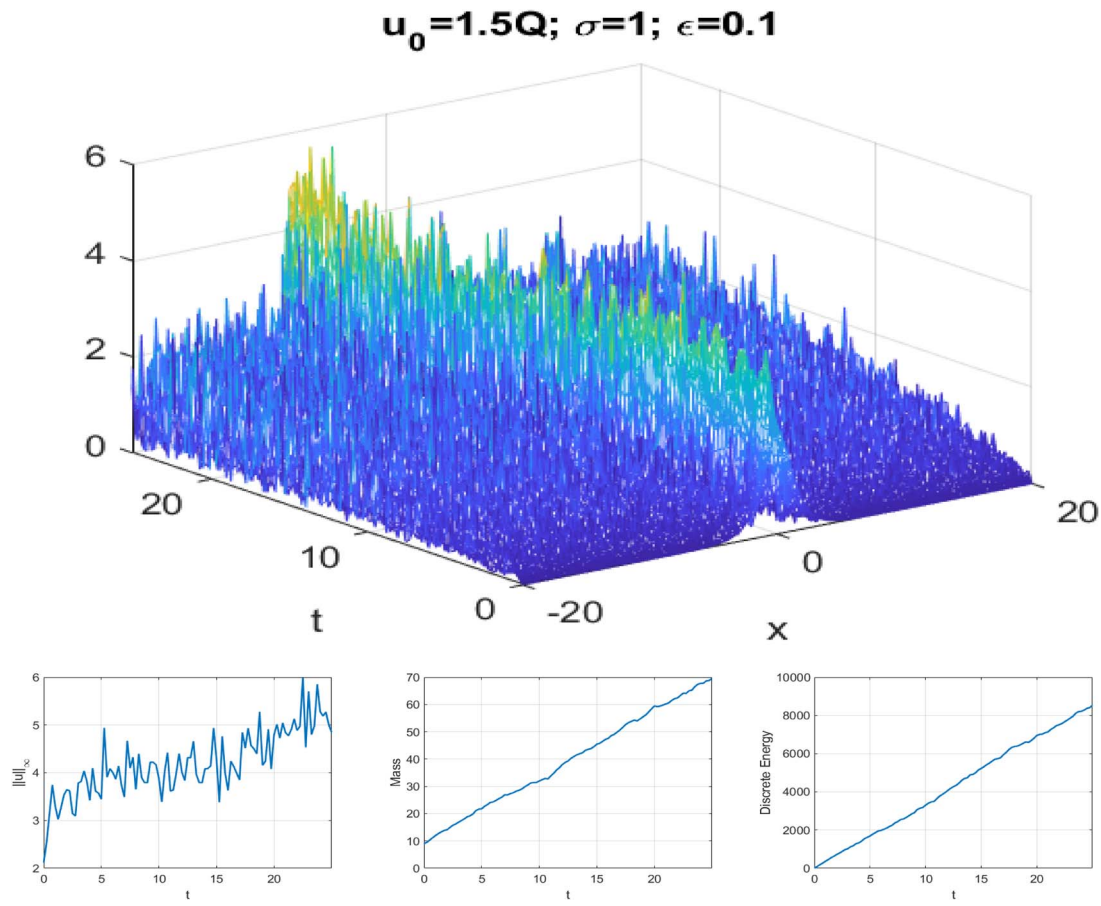

FIG. 16. Additive noise, $\epsilon = 0.1$, $u_0 = 1.5Q$, L^2-subcritical case ($\sigma = 1$). Top: time evolution of $|u(x,t)|$. Bottom: time dependence of $\|u(t)\|_\infty$, mass and energy.

with slow increase of the L^∞ norm and linearly growing mass and energy. Since it is a sub-critical case, the blow up will not happen (e.g. Weinstein, 1987, or de Bouard & Debussche, 2002b). Figure 16 shows that the $\|u\|_\infty$ grows linearly with respect to time. Note that in the subcritical case (when $\delta = 1$) there are globally existing solutions in the deterministic setting. Thus, we conjecture that the solution exists globally in time with an additive noise.

Returning to the L^2-critical and supercritical SNLS, we have seen that even small initial data can lead to blow up. Therefore, we next compute the percentage of solutions that blow up until some finite time (e.g. $t = 5$). We run $N_t = 1000$ trials to track solutions for various values of magnitude A in the initial data $u_0 = A\,Q$, with A close to 1. In Table 1, we show the percentage of finite time blow-up solutions in the L^2-critical case ($\sigma = 2$) with an additive noise ($\epsilon = 0.01, 0.05, 0.1$): we take $A = 0.95, 1$ and 1.05 (in the deterministic case, these amplitudes would, respectively, lead to a scattering solution, a soliton and a finite-time blow up). Observe that blow up occurs for $t < 5$ even when $A = 0.95 < 1$ with strong enough noise (e.g. when $\epsilon = 0.1$, we get 98.4% of all solutions blow up in finite time; with

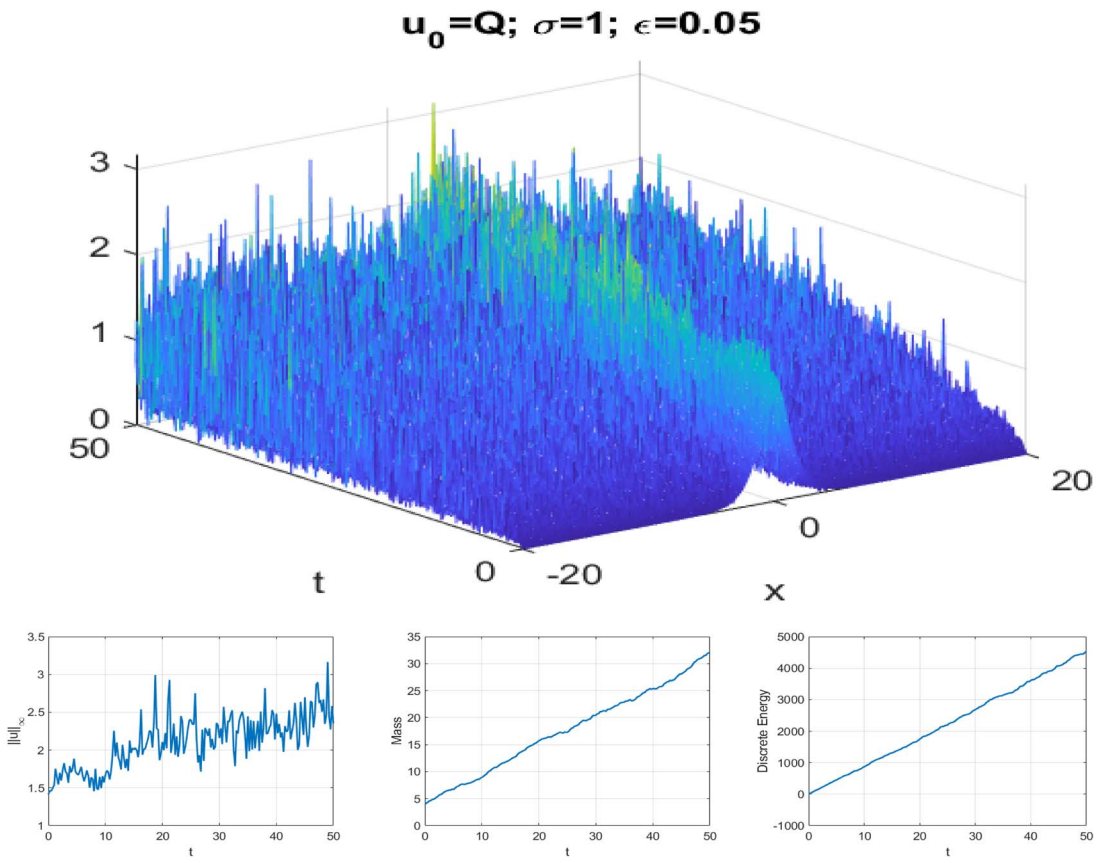

FIG. 17. Additive noise, $\epsilon = 0.1$, $u_0 = Q$, L^2-subcritical case ($\sigma = 1$). Top: time evolution of $|u(x,t)|$. Bottom: time dependence of $\|u(t)\|_{L^\infty}$, mass and energy.

$\epsilon = 0.05$, we get 2.8% blow-up solutions, see Table 1). This is in contrast with multiplicative noise as well as with the deterministic case in the L^2-critical setting.

Table 2 shows the percentage of blow-up solutions in the L^2-supercritical case ($\sigma = 3$) with additive noise. As in the L^2-critical case, solutions with an amplitude below the threshold (e.g. $A = 0.95$) can blow up in finite time (here, before $t = 5$) with an additive noise of larger strength (e.g. when $\epsilon = 0.05$, 3% of our runs blow up in finite time; for $\epsilon = 0.1$ it is 98.6%).

The effect of driving a time evolution into the blow-up regime (or in other words, generating a blow up in the cases when a deterministic solution would exist globally and scatter) might be more obvious in the additive case, since the noise simply adds into the evolution and does not interfere with the solution. What happens in the multiplicative case, since the noise is being multiplied by the solution, is less obvious. Therefore, for completeness, we mention the number of blow-up solutions we observe with $A < 1$ in the multiplicative case. We tested the L^2-supercritical case with $\epsilon = 0.1$ for a multiplicative perturbation and observed the following: for $\sigma = 3$, $u_0 = 0.99\,Q$, the number $N_t = 50\,000$ trial runs produced 2 blow-up trajectories. Thus, while the probability of (specific) finite time blow up is extremely small (in this case it is 0.004%), it is nevertheless positive. The positive probability of blow

up in the L^2-supercritical case is consistent with theoretical results of de Bouard & Debussche (2005), which showed that in such a case any data will lead to blow up in any given finite time with positive probability.

In the L^2-critical case, it was shown in Millet & Roudenko (2021, Theorem 2.7) that if $\|u_0\|_{L^2} < \|Q\|_{L^2}$, then in the multiplicative (Stratonovich) noise case, the solution $u(t)$ is global, thus, no blow up occurs. We tested the initial condition $u_0 = 0.99\,Q$, $\epsilon = 0.1$ (same as in the L^2-supercritical case), and ran again $N_t = 50\,000$ trials. In all cases, we obtained scattering behaviour (or no blow-up trajectories), thus confirming the theory.

We next show how the blow-up solutions form and their dynamics in both cases of noise.

6. Blow-up dynamics

In this section, we study the blow-up dynamics and how it is affected by the noise. We continue applying the numerical algorithms introduced in Section 3. We start with the L^2-critical case and then continue with the L^2-supercritical case. We first observe that, as the blow up starts forming, there is less and less effect of the noise on the blow-up profile and almost no effect on the the blow-up rate. However, we do notice that the noise shifts the 'location' of the blow-up centre slightly for different trial runs.

In order to better understand the blow-up behaviour (and track profile, rate, location), we run 1000 simulations and then average over all runs. For the location of the blow up, we show the distribution of the location of the blow-up centre shifts and its dependence on the number of runs. When using a very large number of trials, we obtain a normal distribution, see Figs 21 and 27. For more details on the blow-up dynamics in the deterministic case, we refer the reader to Yang *et al.* (2018), Yang *et al.* (2019), Sulem & Sulem (1999) and Fibich (2015).

6.1 *The L^2-critical case*

We first consider the quintic NLS ($\sigma = 2$) and $\epsilon = 0$ (deterministic case) and then $\epsilon = 0.01, 0.05$ and 0.1 with a multiplicative noise. We use generic Gaussian initial data ($u_0 = Ae^{-x^2}$) as well as the ground state data ($u_0 = AQ$). Figure 18 shows the blow-up dynamics of $u_0 = 3e^{-x^2}$ with $\epsilon = 0.1$. Observe that the solution slowly converges to the rescaled ground state profile Q. Similar convergence of the profiles for other values of ϵ is observed (we also tested $\epsilon = 0.01$ and 0.05 and compared with our deterministic work $\epsilon = 0$ in Yang *et al.*, 2018). The last (right bottom) subplot on Fig. 18 shows that indeed the profile of blow-up approaches the rescaled Q; however, one may notice that it converges slowly (compare this with the supercritical case in Fig. 24). This confirms the profile in Conjecture 1.

We next study the rate of the blow up by checking the dependence of $L(t)$ on $T - t$. In Fig. 19, we show the rate of blow up on the logarithmic scale. Note that the slope in the linear fitting in each case is $\frac{1}{2}$, thus confirming the rate in Conjecture 1, $\|\nabla u(t)\|_{L^2} \sim (T-t)^{-\frac{1}{2}}$, possibly with some correction terms. This is similar to the deterministic L^2-critical case; see more on that in Sulem & Sulem (1999) and Yang *et al.* (2018).

To provide a justification towards the claim that the correction in the stochastic perturbation case is also of a 'log-log' type, see (1.9), we track similar quantities as we did in the dynamic rescaling method for the deterministic NLS-type equations; see Yang *et al.* (2018), Yang *et al.* (2019) and Yang *et al.* (2020). We track the quantity $a(t) = -LL_t$, or equivalently, in the rescaled time $\tau = \int_0^t \frac{1}{L(s)^2}\,\mathrm{d}s$ (or $\frac{d\tau}{dt} = \frac{1}{L^2(t)}$), we have $a(\tau) = -\frac{L_\tau}{L}$. In the discrete version, by setting $\Delta\tau = \Delta t_0$, we get $\tau_m = m \cdot \Delta t_0$

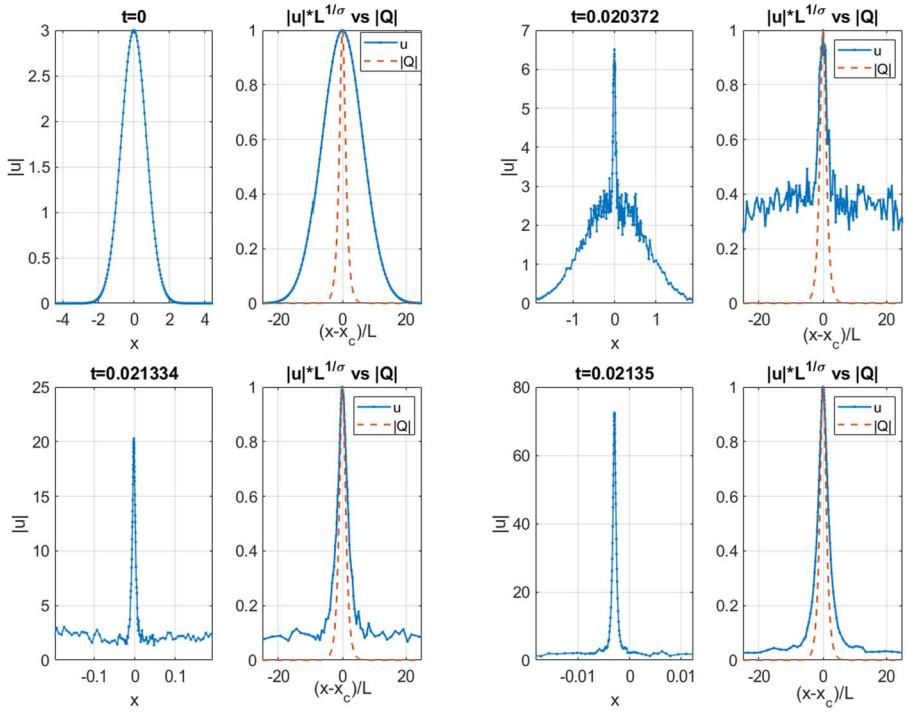

FIG. 18. Multiplicative noise, $\epsilon = 0.1$. Formation of blow up in the L^2-critical case ($\sigma = 2$): snapshots of a blow-up solution (given in pairs of actual and rescaled solution) at different times. Each pair of graphs shows in blue the actual solution $|u|$ and its rescaled solution $L^{1/\sigma}|u|$, which is compared to the absolute value of the normalized ground state solution $e^{it}Q$ in dashed red.

as a rescaled time. Consequently, at the mth step, we have $L(\tau_m)$, $u(\tau_m)$ and $a(\tau_m)$. As in Sulem & Sulem (1999), Fibich (2015) and Yang *et al.* (2018), the parameter a can be evaluated by setting $L(t) = \left(1/\|\nabla u(t)\|_{L^2}\right)^{\frac{2}{\alpha}}$ with $\alpha = 1 + \frac{2}{\sigma} = 2 - 2s$, since $s = \frac{1}{2} - \frac{1}{\sigma}$. Then, similar to Sulem & Sulem (1999, Chapter 6), we get

$$a(t) = -\frac{2}{\alpha} \frac{1}{(\|\nabla u(t)\|_{L^2}^2)^{\frac{2}{\alpha}+1}} \int |u|^{2\sigma} \operatorname{Im}(u_{xx}\bar{u})\, \mathrm{d}x. \tag{6.1}$$

Here, we specifically write a more general statement in terms of the dimension d and nonlinearity power $\sigma \searrow 2$, since the convergence of those parameters down to $d = 1$ and $\sigma = 2$ is crucial in determining the correction in the blow-up rate (see more in Yang *et al.*, 2018), as well as the value of $a(\tau)$ for the profile identification in the supercritical case. The integral in (6.1) is evaluated by the composite trapezoid rule.

Figure 20 shows the dependence of the parameter a with respect to $\log L$ for a single trajectory (in dotted red) and for the averaged value over 2400 runs (in solid blue) on the left subplot (the strength of the multiplicative noise is $\epsilon = 0.1$). Observe that a single trajectory gives a dependence with severe oscillations due to noise in the beginning but eventually smoothes out and converges to the average value as it approaches the blow-up time T. This matches our findings in Fig. 18, where eventually the blow-up profile becomes smooth.

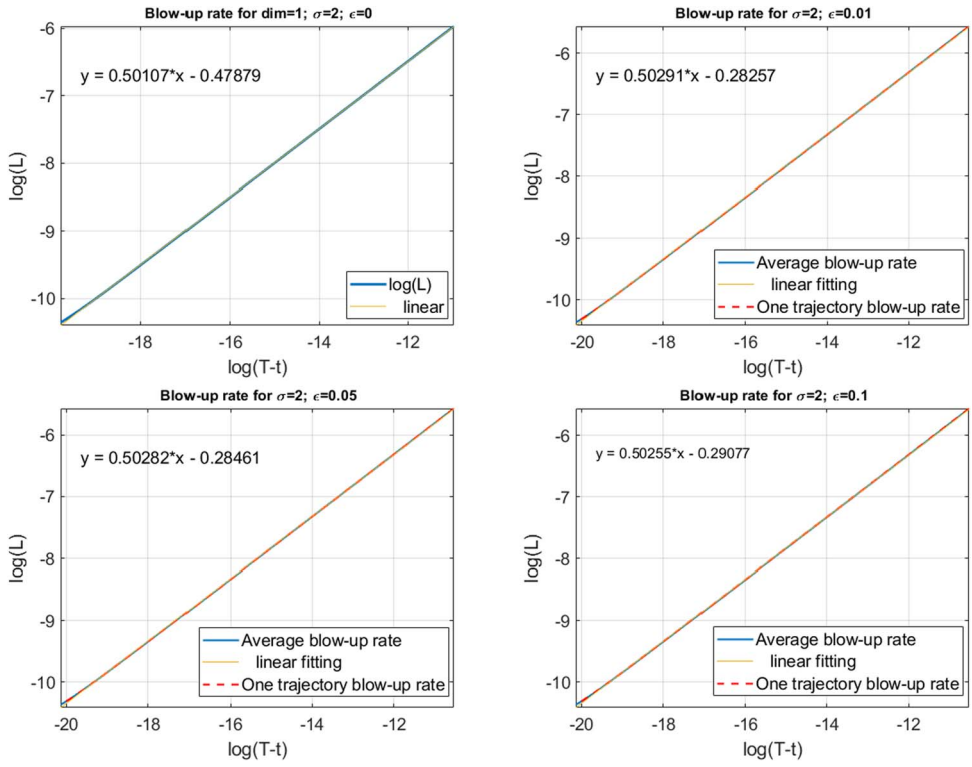

FIG. 19. Multiplicative noise, L^2-critical case. The fitting of the rate $L(t)$ v.s. $(T-t)$ on a log scale. The values of the noise strength ϵ are 0 (top left), 0.01 (top right), 0.05 (bottom left) and 0.1 (bottom right). Observe that in all cases the linear fitting gives the slope 0.50.

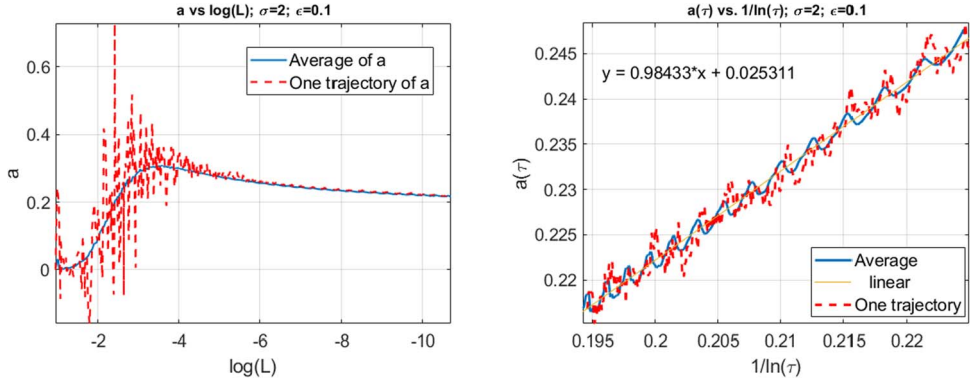

FIG. 20. Multiplicative noise, $\epsilon = 0.1$, L^2-critical case. Left: a vs. $\log(L)$. Right: linear fitting for $a(\tau)$ vs. $1/\ln(\tau)$.

The right subplot shows the linear fitting for $a(\tau)$ vs. $1/\ln(\tau)$. One may notice small oscillations in the blue curve: perhaps with the increase of the number of runs, the blue curve could have smaller and smaller oscillations and would eventually approach a (yellow) line. We show one trajectory dependence

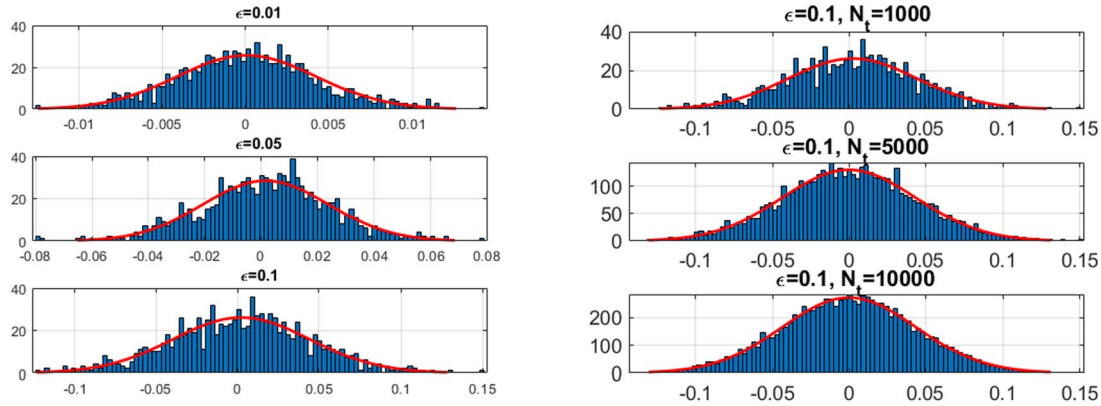

FIG. 21. Multiplicative noise, $\epsilon = 0.1$, L^2-critical case. Left: shifts x_c of the blow-up centre for different noise strength ϵ with the fixed $N_t = 1000$ number of runs. Right: dependence of shifts on the number of runs N_t for the same $\epsilon = 0.1$; observe that it approaches the normal distribution as the number of runs increases.

TABLE 3 *Multiplicative noise. The variance of the blow-up centre shifts x_c in $N_t = 1000$ trials, see also Fig. 21*

ϵ	0.01	0.05	0.1
$\sigma = 2$ (L^2-critical)	$1.75e-5$	$5.0e-4$	0.0018
$\sigma = 3$ (L^2-supercritical)	0.0025	0.0043	0.0060

in dotted red, the averaged value in solid blue and the linear fitting in solid yellow. This gives us first confirmation that the correction term is of logarithmic order. As in the deterministic case, we suspect that the correction is a double logarithm; however, this will require further investigations, which are highly non-trivial (even in the deterministic case). The above confirms Conjecture 1 up to one logarithmic correction.

6.1.1 *Blow-up location.* So far we exhibited similarities in the blow-up dynamics between the multiplicative noise case and the deterministic case. A feature, which we find different, is the location of blow up. We observe that the blow-up core, to be precise the spatial location x_c of the blow-up 'centre', shifts away from the zero (or rather wanders around it) for different runs. We record the values x_c of shifts and plot their distribution in Fig. 21 for various values of ϵ and for different number of trials N_t to track the dependence.

Our first observation is that the centre shifts further away from zero when the strength of noise ϵ increases. Secondly, we observe that the shifting has a normal distribution (see the right bottom subplot with the maximal number of trials in Fig. 21). The mean of this distribution approaches 0 when the number of runs N_t increases. We record the variance of the shifts for different ϵs and σs in Table 3. The variance seems to be an increasing function of the strength of the noise, which confirms our first observation above. In the same table, we also record the L^2-supercritical case that is discussed later.

The Kolmogorov–Smirnov test verifies our assumption. We renormalize the observations of x_c subtracting the empirical mean and dividing by the empirical standard deviation to check that the distribution is that of a standard Gaussian. The outcome of the Kolmogorov–Smirnov test is to accept

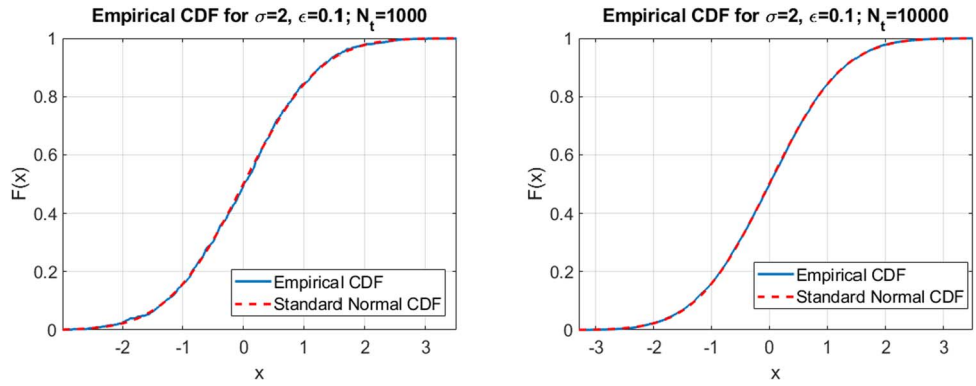

FIG. 22. Multiplicative noise in the L^2-critical case, $\epsilon = 0.1$. Comparison between the empirical CDF for the location of x_c (solid blue) and the standard normal CDF (red dash). Left: $N_t = 1000$. Right: $N_t = 10000$.

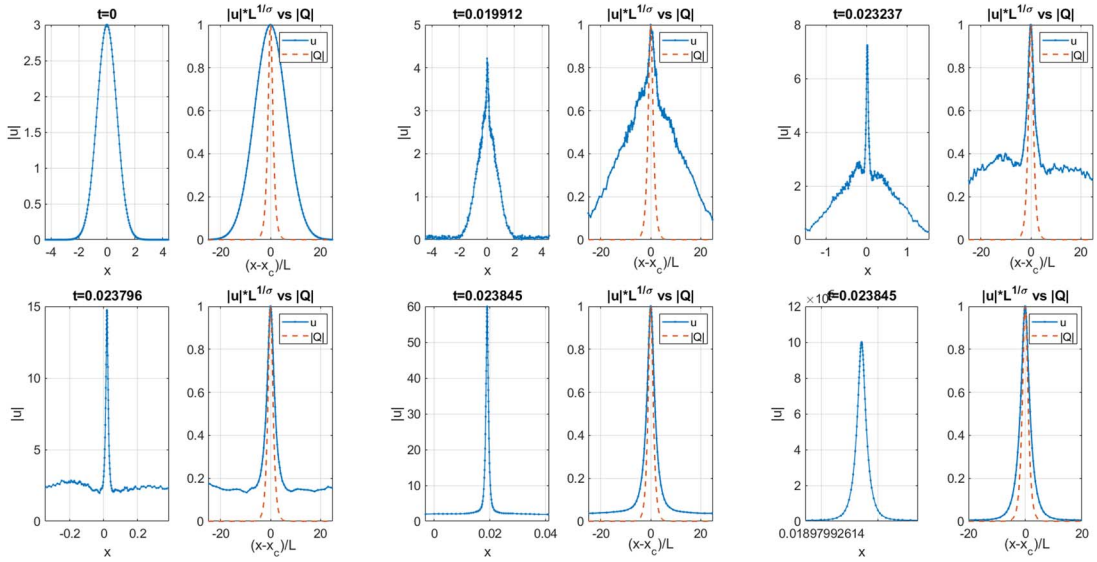

FIG. 23. Additive noise, $\epsilon = 0.1$. Formation of blow up in the L^2-critical case ($\sigma = 2$): snapshots of a blow-up solution at different times.

the $N(0,1)$ hypothesis against the alternative at the 5% significance level. The test is based on the comparison of empirical and theoretical cumulative distribution functions (CDFs). Figure 22 shows the comparison between the empirical CDF of the renormalized blow-up centre x_c (blue solid line) and the $N(0,1)$ standard normal CDF (red dash). The left subplot shows the case for $N_t = 1000$ and the right subplot is the case for $N_t = 10000$ when $\epsilon = 0.1$. We omit the results for other values of ϵ since they are similar.

In the case of an additive noise, we obtain analogous results; for brevity, we only include Fig. 23 to show convergence of the profiles, the other features remain similar and we omit them.

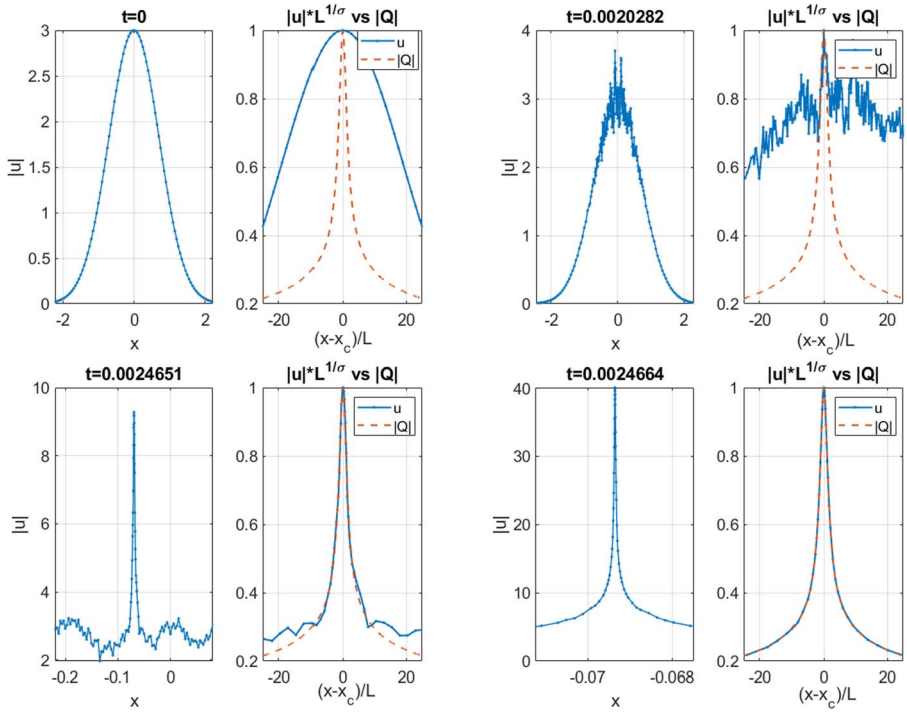

FIG. 24. Multiplicative noise, $\epsilon = 0.1$. Formation of blow up in the L^2-supercritical case ($\sigma = 3$): snapshots at different times: the actual solution (blue) compared to the rescaled profile $Q_{1,0}$ (red). Note a visibly perfect match in the last right bottom subplot.

We conclude that in the L^2-critical case, regardless of the type of stochastic perturbation (multiplicative or additive) and the strength (different values of ϵ) of the noise, the solution always blows up in a self-similar regime with the rescaled profile of the ground state Q and the square root blow-up rate with the logarithmic correction, thus confirming Conjecture 1.

6.2 *The L^2-supercritical case*

In the L^2-supercritical case, we consider the septic NLS equation ($\sigma = 3$) as before with multiplicative or additive noise. We use either Gaussian-type initial data $u_0 = A\,e^{-x^2}$ or a multiple of the ground state solution $u_0 = AQ$, where Q is the ground state solution with $\sigma = 3$ in (1.4). We consider the multiplicative noise of strength $\epsilon = 0.01, 0.02$ and 0.1 and investigate the blow-up profile. For the initial data $u_0 = 3\,e^{-x^2}$, Fig. 24 shows the solution profiles at different times for $\epsilon = 0.1$. The two main observations are the following: (i) the solution smoothes out faster compared to the L^2-critical case (see Fig. 18); (ii) it converges to a self-similar profile very fast. To confirm this, we compare the bottom right subplots in both Fig. 18 and Fig. 24: in the supercritical case, the profile of the rescaled solution (in solid blue) practically coincides with the absolute value of the renormalized $Q \equiv Q_{1,0}$ (in dashed red); this is similar to the deterministic case.

Tests of other data and various values of ϵ show that all observed blow-up solutions converge to the profile $Q_{1,0}$. In Fig. 25, we show the linear fitting for the log dependence of $L(t)$ vs. $(T-t)$, which gives

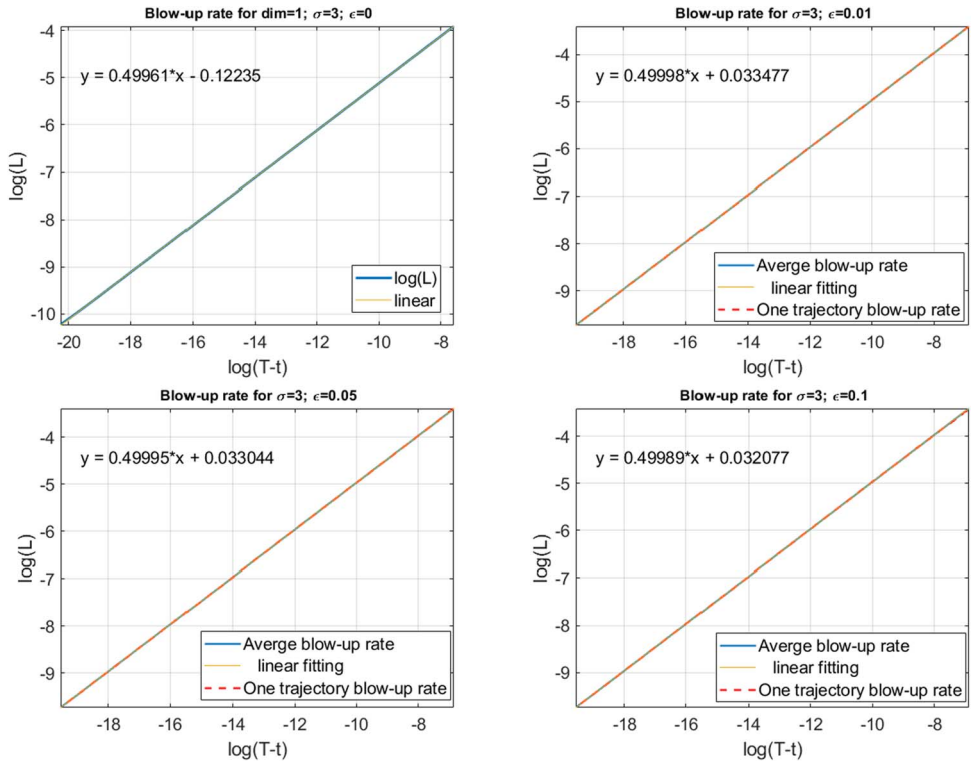

FIG. 25. Multiplicative noise, L^2-supercritical case. A linear fitting of the rate $L(t)$ vs. $(T-t)$ on log scale. The values of the noise strength ϵ are 0 (top left), 0.01 (top right), 0.05 (bottom left) and 0.1 (bottom right); the linear fitting gives 0.50 slope.

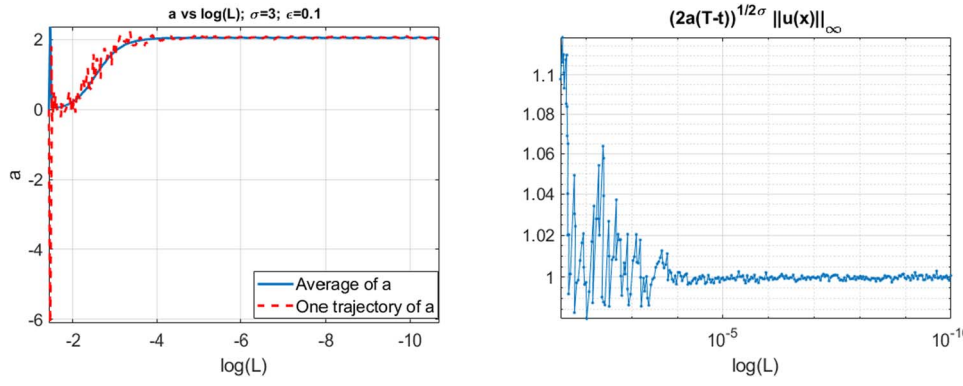

FIG. 26. Multiplicative noise, L^2-supercritical case, $\epsilon = 0.1$. Left: a vs. $\log(L)$, the focusing level. Right: numerical confirmation of the blow-up rate $\|u(t)\|_\infty = (2a(T-t))^{-\frac{1}{2\sigma}}$ (the limit has stabilized at 1).

the slope $\frac{1}{2}$. Note that even one trajectory fitting is very good. Further justification of the blow-up rate is done by checking the behaviour of the quantity $a(\tau)$ from (6.1). Figure 26 shows that the quantity $a(\tau)$

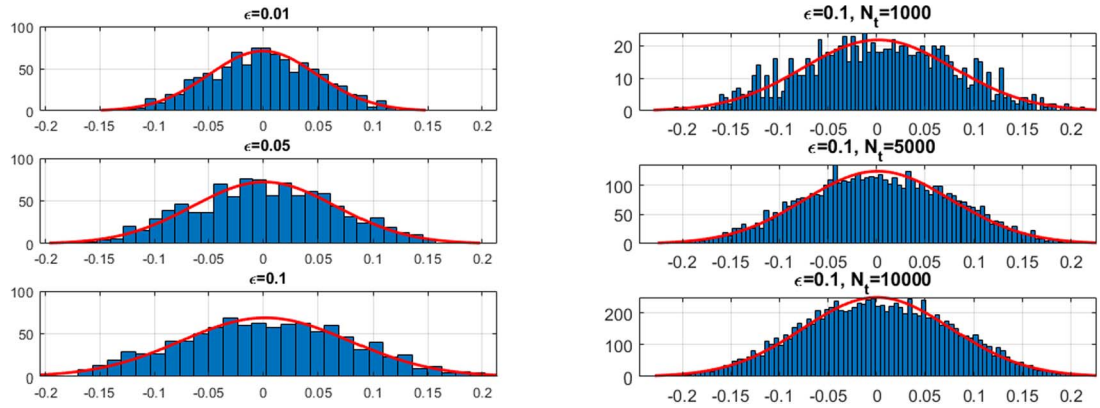

FIG. 27. Multiplicative noise, L^2-supercritical case. Left: distribution of shifts x_c of the blow-up centre for different ϵs with $N_t = 1000$ runs. Right: as N_t increases, it becomes more evident that the spread out of the blow-up location satisfies a normal distribution.

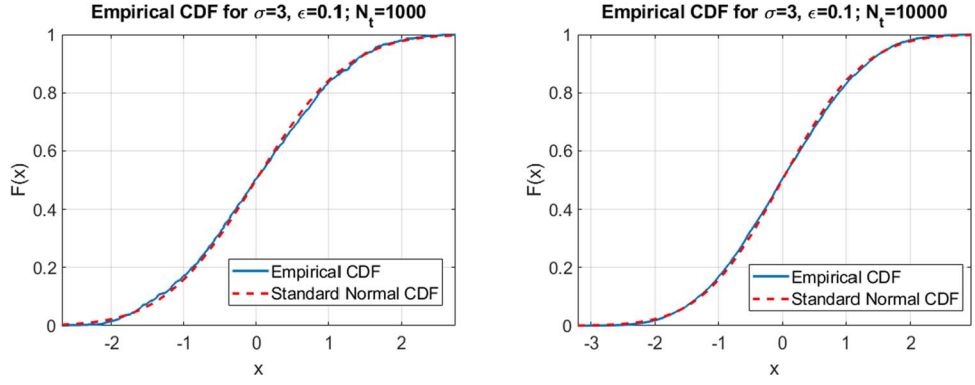

FIG. 28. Multiplicative noise in the L^2-supercritical case, $\epsilon = 0.1$. Comparison between the empirical CDF for the location of x_c (solid blue) and the standard normal CDF (red dash). Left: $N_t = 1000$. Right: $N_t = 10000$.

converges to a constant very fast (comparing with the decay to zero of $a(\tau)$ in the L^2-critical case in Fig. 25). Since $a(t) \to a$, a constant, we have $a = -LL_t$ and solving this ODE (with $L(T) = 0$) yields

$$L(t) = \sqrt{2a(T-t)}.$$

Recall that $L(t) = \left(1/\|\nabla u(t)\|_{L^2}\right)^{\frac{2}{\alpha}}$, or equivalently, $L(t) = 1/\|u(t)\|_\infty^\sigma$; thus, we have the blow-up rate (1.11) for the supercritical case, or equivalently,

$$\|u(t)\|_\infty = (2a(T-t))^{-\frac{1}{2\sigma}} \text{ as } t \to T,$$

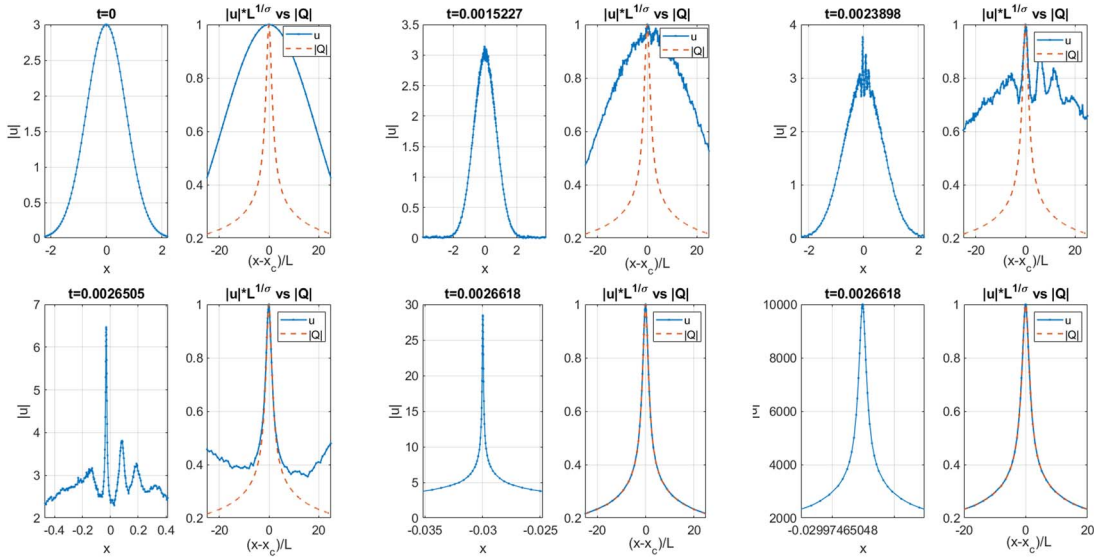

FIG. 29. Additive noise, $\epsilon = 0.1$. Convergence of the blow up in the L^2-supercritical case ($\sigma = 3$); actual solution and its rescaled version (blue), the rescaled profile solution $Q_{1,0}$ (red).

in the case when we evaluate the L^∞ norm. This indicates that solutions blow up with the pure power rate without any logarithmic correction, similar to the deterministic case (for details, see Budd *et al.*, 1999; Yang *et al.*, 2019).

In the L^2-supercritical case, we also observe shifting of the blow-up centre and show the distribution of shifts x_c in the multiplicative noise; in particular, these random shifts have a normal distribution similar to the L^2-critical case. The variance of shifts is shown in Table 3. The Kolmogorov–Smirnov test accepts the hypothesis that the renormalized values of x_c follow a standard Gaussian distribution against the alternative at the 5% significance level. Figure 28 shows the comparison between the empirical CDF (blue solid) and the standard normal CDF (red dash) for $\epsilon = 0.1$. The left subplot is the case for $N_t = 1000$ and the right plot is the case for $N_t = 10000$. One can notice that there is little difference. Again, the right subplot matches the standard normal CDF better as expected. Note that stronger noises (that is, larger values of ϵ) yield a larger shift away from the origin. Furthermore, comparing Table 3, we find that the L^2-supercritical case produces slightly larger variance of shifts than the L^2-critical case. In other words, we observe that higher power of nonlinearity creates a larger variance, i.e. the blow-up location is more spread out.

We obtained similar results in the additive noise: the blow up occurs in a self-similar way at the rate $L(t) = (2a(T-t))^{\frac{1}{2}}$, and the solution profile converges to the profile $Q_{1,0}$ relatively fast, see Fig. 23 for profile convergence. The quantities $a(\tau)$, $L(\tau)$ also behave similar to the multiplicative noise parameters (and also to the deterministic cases). This confirms Conjecture 2.

7. Conclusion

In this work, we investigate the behaviour of solutions to the 1D focusing SNLS subject to a stochastic perturbation which is either multiplicative or additive and driven by space-time white noise. In particular,

we study the time dependence of the mass (L^2-norm) and the energy (Hamiltonian) in the L^2-critical and supercritical cases. For that, we consider a discretized version of both quantities and an approximation of the actual mass or energy. In the deterministic case, these quantities are conserved in time; however, it is not necessarily the case in the stochastic setting. In the case of a multiplicative noise, which is defined in terms of the Stratonovich integral, the mass (both discrete and actual) is invariant. However, in the additive case, the mass grows linearly. The energy grows in time in both stochastic settings. We give upper estimates on that time dependence and then track it numerically; we observe that energy levels off when the noise is multiplicative. We also investigate the dependence of the mass and energy on the strength of the noise, on the spatial and temporal mesh refinements and the length of the computational interval.

For the above, we use three different numerical schemes; all of them conserve discrete mass in the multiplicative noise setting, and one of them conserves the discrete energy in the deterministic setting, though that scheme involves fixed point iterations to handle the nonlinear system, thus taking longer computational time. We introduce a new scheme, a linear extrapolation of the above and CN discretization of the potential term, which speeds up significantly our computations, since the scheme is linear and thus avoiding extra fixed point iterations while having tolerable errors.

We also introduce a new algorithm in order to investigate the blow-up dynamics. Typically in the deterministic setting to track the blow-up dynamics, the dynamic rescaling method is used. We use instead a finite difference method with non-uniform mesh and then mesh-refinement with mass-conservative interpolation. With this algorithm, we are able to track the blow-up rate and profile and we find a new feature in the blow-up dynamics, the shift of the blow-up centre, which follows normal distribution for large number of trials. We note that our algorithm is also applicable for the deterministic NLS equation, in particular, it can replace the dynamic rescaling or moving mesh methods used to track blow up.

We confirm previous results of Debussche & Di Menza (2002b) and de Bouard & Debussche (2002b, 2005) showing that the additive noise can amplify or create blow up (we suspect that this happens almost surely for any data) in the L^2-critical and supercritical cases. In the multiplicative noise setting, the blow up seems to occur for any (sufficiently localized) data in the L^2-supercritical case and above the mass threshold in the L^2-critical case. Finally, when the noise is present, a solution is likely to travel away from the initial 'centre', and, once the solution starts blowing up, the noise plays no role in the singularity structure, and the blow up occurs with the rate and profile similar to the deterministic setting.

Acknowledgements

The authors thank an anonymous referee for suggesting clarifications on blow-up existence time in Section 3, and for valuable comments which helped improve the paper. This work was partially written while the first author visited Florida International University. She would like to thank FIU for the hospitality. A. M.'s research has been conducted within the FP2M federation (CNRS FR 2036).

Funding

United States National Science Foundation (DMS-1815873 and DMS-1927258, the PI: S.R.; postdoctoral researcher: K.Y.).

References

Abdullaev, F. K. & Garnier, J. (2005) Propagation of matter-wave solitons in periodic and random nonlinear potentials. *Phys. Rev. E*, **72**, 061605(R).

Barton-Smith, M., Debussche, A. & Di Menza, L. (2005) Numerical study of two-dimensional stochastic NLS equations. *Numer. Methods Partial Differential Equations*, **21**, 810–842.

de Bouard, A. & Debussche, A. (2002a) Finite-time blow-up in the additive supercritical stochastic nonlinear Schrödinger equation: the real noise case. *The Legacy of the Inverse Scattering Transform in Applied Mathematics (South Hadley, MA, 2001)*. Contemp. Math., vol. 301. Providence, RI: Amer. Math. Soc., pp. 183–194.

de Bouard, A. & Debussche, A. (2002b) On the effect of a noise on the solutions of the focusing supercritical nonlinear Schrödinger equation. *Probab. Theory Related Fields*, **123**, 76–96.

de Bouard, A. & Debussche, A. (2003) The stochastic nonlinear Schrödinger equation in H^1. *Stochastic Anal. Appl.*, **21**, 97–126.

de Bouard, A. & Debussche, A. (2005) Blow-up for the stochastic nonlinear Schrödinger equation with multiplicative noise. *Ann. Probab.*, **33**, 1078–1110.

Budd, C. J., Chen, S. & Russell, R. D. (1999) New self-similar solutions of the nonlinear Schrödinger equation with moving mesh computations. *J. Comput. Phys.*, **152**, 756–789.

Cazenave, T. (2003) *Semilinear Schrödinger Equations*. Courant Lecture Notes in Mathematics, vol. 10. New York: New York University, Courant Institute of Mathematical Sciences; Providence, RI: American Mathematical Society.

Cazenave, T. & Weissler, F. B. (1990) The Cauchy problem for the critical nonlinear Schrödinger equation in H^s. *Nonlinear Anal.*, **14**, 807–836.

Debussche, A. & Di Menza, L. (2002a) Numerical resolution of stochastic focusing NLS equations. *Appl. Math. Lett.*, **15**, 661–669.

Debussche, A. & Di Menza, L. (2002b) Numerical simulation of focusing stochastic nonlinear Schrödinger equations. *Phys. D*, **162**, 131–154.

Dodson, B. (2015) Global well-posedness and scattering for the mass critical nonlinear Schrödinger equation with mass below the mass of the ground state. *Adv. Math.*, **285**, 1589–1618.

Duyckaerts, T., Holmer, J. & Roudenko, S. (2008) Scattering for the non-radial 3D cubic nonlinear Schrödinger equation. *Math. Res. Lett.*, **15**, 1233–1250.

Falkovich, G. E., Kolokolov, I., Lebedev, V. & Turitsyn, S. K. (2001) Statistics of soliton-bearing systems with additive noise. *Phys. Rev. E*, **63**, 025601(R).

Fang, D., Xie, J. & Cazenave, T. (2011) Scattering for the focusing energy-subcritical nonlinear Schrödinger equation. *Sci. China Math.*, **54**, 2037–2062.

Fibich, G. (2015) *The nonlinear Schrödinger Equation: Singular Solutions and Optical Collapse*. Applied Mathematical Sciences, vol. 192. Cham: Springer, pp. xxxii+862.

Garnier, J. (1998) Asymptotic transmission of solitons through random media. *SIAM J. Appl. Math*, **58**, 1969–1995.

Ginibre, J. & Velo, G. (1979) On a class of nonlinear Schrödinger equations. I. The Cauchy problem, general case. *J. Funct. Anal.*, **32**, 1–32.

Ginibre, J. & Velo, G. (1985) The global Cauchy problem for the nonlinear Schrödinger equation revisited. *Ann. Inst. Henri Poincaré Anal. Non Linéaire*, **2**, 309–327.

Guevara, C. D. (2014) Global behavior of finite energy solutions to the d-dimensional focusing nonlinear Schrödinger equation. *Appl. Math. Res. Express. AMRX*, 177–243. 10.1002/cta.2381.

Holmer, J. & Roudenko, S. (2007) On blow-up solutions to the 3D cubic nonlinear Schrödinger equation. *Appl. Math. Res. Express. AMRX*, Art. ID abm004, 31.

Holmer, J. & Roudenko, S. (2008) A sharp condition for scattering of the radial 3D cubic nonlinear Schrödinger equation. *Comm. Math. Phys.*, **282**, 435–467.

Holmer, J. & Roudenko, S. (2010) Divergence of infinite-variance nonradial solutions to the 3D NLS equation. *Comm. Partial Differential Equations*, **35**, 878–905.

Holte, J. M. (2009) Discrete Gronwall lemma and applications. *MAA North Central Section Meeting at Univ North Dakota*, (Oct 24), 1–8.

Kato, T. (1987) On nonlinear Schrödinger equations. *Ann. Inst. H. Poincaré Phys. Théor.*, **46**, 113–129.

KENIG, C. E. & MERLE, F. (2006) Global well-posedness, scattering and blow-up for the energy-critical, focusing, non-linear Schrödinger equation in the radial case. *Invent. Math.*, **166**, 645–675.

KOPELL, N. & LANDMAN, M. (1995) Spatial structure of the focusing singularity of the nonlinear Schrödinger equation: a geometrical analysis. *SIAM J. Appl. Math.*, **55**, 1297–1323.

LEMESURIER, B., PAPANICOLAOU, G., SULEM, C. & SULEM, P.-L. (1987) The focusing singularity of the nonlinear Schrödinger equation. *Directions in Partial Differential Equations (Madison, WI, 1985)*. Publ. Math. Res. Center Univ. Wisconsin, vol. 54. Boston, MA: Academic Press, pp. 159–201.

LIFSHITS, M. (2012) *Lectures on Gaussian Processes*. Springer Briefs in Mathematics. Springer.

MERLE, F. (1993) Determination of blow-up solutions with minimal mass for nonlinear Schrödinger equations with critical power. *Duke Math. J.*, **69**, 427–454.

MERLE, F. & RAPHAEL, P. (2005a) The blow-up dynamic and upper bound on the blow-up rate for critical nonlinear Schrödinger equation. *Ann. of Math. (2)*, **161**, 157–222.

MERLE, F. & RAPHAEL, P. (2005b) Profiles and quantization of the blow up mass for critical nonlinear Schrödinger equation. *Comm. Math. Phys.*, **253**, 675–704.

MILLET, A. & ROUDENKO, S. (2021) Well-posedness for the focusing stochastic critical and supercritical nonlinear Schrödinger equaion, *Preprint*.

PERELMAN, G. (2000) Evolution of adiabatically perturbed resonant states. *Asymptot. Anal.*, **22**, 177–203.

RASMUSSEN, K., GAIDIDEI, Y., BANG, O. & CHRISTIANSEN, P. (1995) The influence of noise on critical collapse in the nonlinear Schrödinger equation. *Phys. Rev. A*, **204**, 121–127.

SULEM, C. & SULEM, P.-L. (1999) *The Nonlinear Schrödinger Equation: Self-focusing and Wave Collapse*. Applied Mathematical Sciences, vol. 139. New York: Springer.

TSUTSUMI, Y. (1987) L^2-solutions for nonlinear Schrödinger equations and nonlinear groups. *Funkcial. Ekvac.*, **30**, 115–125.

VLASOV, S., PETRISHCHEV, L. & TALANOV, V. (1970) Averaged description of wave beams in linear and nonlinear media (the method of moments). *Radiophys. Quantum Electron.*, **14**, 1062–1070. Translated from *Izv. Vyssh. Uchebn. Zaved. Radiofiz.*, **14**, 1253–1263.

WEINSTEIN, M. I. (1982/83) Nonlinear Schrödinger equations and sharp interpolation estimates. *Comm. Math. Phys.*, **87**, 567–576.

WEINSTEIN, M. I. (1987) Solitary waves of nonlinear dispersive evolution equations with critical power nonlinearities. *J. Differential Equations*, **69**, 192–203.

YANG, K., ROUDENKO, S. & ZHAO, Y. (2018) Blow-up dynamics and spectral property in the L^2-critical nonlinear Schrödinger equation in high dimensions. *Nonlinearity*, **31**, 4354–4392.

YANG, K., ROUDENKO, S. & ZHAO, Y. (2019) Blow-up dynamics in the mass super-critical NLS equations. *Phys. D*, **396**, 47–69.

YANG, K., ROUDENKO, S. & ZHAO, Y. (2020) Stable blow-up dynamics in the L^2-critical and L^2-supercritical generalized Hartree equation. *Stud. Appl. Math.*, **145**, 647–695.

ZAKHAROV, V. E. (1972) Collapse of Langmuir waves. *Sov. Phys. JETP*, **48**, 908–914.